

Reconstruction of Holocene relative sea-level from beach ridges of the central west coast of India using GPR and OSL dating

Pankaj Prasad^{1*}, Victor Joseph Loveson¹, Vinayak Kumar², Anil Dutt Shukla², Priyankar Chandra³, Swati Verma¹, Ramanand Yadav^{1,4}, Rajni Magotra¹, Gurudas M Tirodkar¹

¹Geological Oceanography Division, CSIR- National Institute of Oceanography, Dona Paula 403004, Goa, India

²Planetary and Geosciences Division, Physical Research Laboratory, Navrangpura, Ahmedabad 380009, India

³Department of Geography, Institute of Science, Banaras Hindu University, Varanasi-221005, Uttar Pradesh, India

⁴Department of Geology, The M.S. University of Baroda, Vadodara-390002, India

***Corresponding Author:** Pankaj Prasad

Email: ppankaj.earthscience@gmail.com

Mobile No.: +919883329432

Abstract

The Holocene sea-level and associated shoreline regression of beach ridges in the central west coast of India have been reconstructed based on internal sedimentary architecture and luminescence chronology. For this purpose, various techniques namely ground penetrating radar (GPR), optically-stimulated luminescence (OSL) dating, and interferometry synthetic aperture radar (InSAR) have been used. The berm and beach-dune boundary of paleo beach ridges have been mapped from the high-resolution sub-surface images and converted into sea-level indicators using modern analogs and OSL ages. GPR reflection data shows a number of the seaward dipping radar facies with a few landward dipping facies in paleo beach ridges. In the case of swale, radar signal has been highly attenuated due to the presence of water and mud causing the appearance of multiple horizontal and parallel positive and negative couplets in the sedimentary layer. The results of the research reveal that the oldest beach ridge was formed around 7.7 kyr BP and sea-level was +2 m above mean sea-level. The average progradation rate of these ridges is 0.14 m/yr. From the grain size analysis, it has been found that the larger share of grain size falls into the classes of fine and moderate sand. The present displacement map of the region which has been generated from the Sentinel-1 datasets, demonstrates the average upliftment is 2.5 mm/yr whereas subsidence is 1 mm/yr. The fall of the Holocene relative sea-level with respect to the study region is the consequence of both global and regional events.

Keywords :- Beach ridge; Central west coast of India; Holocene relative sea-level; Sedimentary architecture; GPR; InSAR

1. Introduction

Ridge and swale topography are the prominent depositional landforms along the prograding coasts throughout the world (Wells, 1996; Neal et al., 2003; Clemmensen et al., 2012; Alappat et al., 2015). A beach ridge is defined as a linear mound-shaped ridge, parallel or semi-parallel to the coast that is originated in the intertidal or supratidal zones by coastal and aeolian processes (Otvos, 2000; Neal et al., 2003; Kunte and Wagle, 2005; Clemmensen and Nielsen, 2010). On the other side, swale is defined as an elongated, relatively narrow depression between two beach ridges (Snead, 1982; Otvos, 2000; Clemmensen et al., 2012). The origin and evolution of beach ridges have been studied in detail by Tanner, (1995); Taylor and Stone, 1996; Otvos, (2000); and Tamura, (2012). The number of beach ridges varies from one geographic region to another depending on geological and geomorphological processes. Each beach ridge reflects the position of the paleoshoreline and the associated sea-level. Well-preserved beach ridges record the past relative sealevels, paleoclimatic conditions, catastrophic events, and morpho-dynamics of the region because they respond dynamically to climate change and sea-level fluctuations (Kunte and Wagle, 2005; Storms and Kroonenberg, 2007; Tamura, 2012; Choi et al., 2014). The changes in relative sealevel in a small geographic area are mostly brought about by both global and local conditions such as changes in ice sheets, glacio-isostatic adjustment, tectonic instability (emergence or submergence), coastal configuration changes, sediment deposition, and thermal expansion of the ocean (Taylor and Stone, 1996; Hede et al., 2015; Banerji et al., 2015; Sharma et al., 2021; AlMikhlafi., et al 2021). In regional scale, the records of the Holocene sea-level are not concluded without the knowledge of geological, geomorphological, and tectonic settings of the coastal sector (Williams et al., 1998). Although the RSL reconstruction should be conducted on local scale, the study of sea-level change in regional scale is also meaningful (Hashimi et al., 1995; Li et al., 2012; Sharma et al., 2021). The sea-level change and coastal response during the Holocene have been described by many researchers (Wang et al., 2012, 2013; Xiong et al., 2018). In South and Southeast Asia, the Holocene relative sea-level changes were mainly influenced by global and local drivers like tectonic uplift, subsidence and compaction (Mann et al., 2019). Based on geomorphological and tectonic features on satellite and aerial photos, Ramaswamy, (1989) revealed that the evolution of the Indian coastline has been mainly controlled by tectonism. The neotectonic effects in western India have been discussed in the study of Jain et al. (1998) and Bhattacharya, (2021). On the west coast of India, eustatic sea-level rise and regional neotectonic effects are the main cause of relative sea-level change (Pant and Juyal, 1993; Banerji et al., 2015; Alappat et al., 2015; Sharma et al., 2021). The beach ridges of the west coast of India are of very recent origin, not older than the Holocene age (Kunte and Wagle, 2005). These beach ridges produce the inventory of the Holocene sea-level changes. At

present, global warming and resultant sea-level rise have been a matter of constant debate and are intriguing to study past climate conditions. In this context, it is necessary to develop the knowledge of measuring the paleo sealevel variation to understand and predict future sea-level. Many researchers have attempted to show the effect of relative sea-level changes on the environment and humankind (Shennan, 1986; Khan et al., 2002; Trenhaile, 2010).

In earlier studies, the identification of beach ridges was mainly based on the extensive field survey. With respect to time and cost, this method is no longer desirable in a larger area. It stands in contrast with the nowadays medium to high-resolution satellite images which help immensely to demarcate the beach ridges in a greater area minimizing time and cost (Loveson, and Rajamanickam, 1994). However, remote sensing technique does not provide in-depth information on beach ridges. For that, knowledge of internal architecture and stratigraphic pattern of the beach ridges is required to reconstruct the paleo-environment of the region (Neal et al., 2003; Nielsen and Clemmensen, 2009; Clemmensen et al., 2012; Houser, 2012; Lindhorst and Schutter, 2014; Hede et al., 2015; Nielsen et al., 2017). Among the methods, GPR is a non-invasive geophysical technique that allows collecting the high-resolution detailed subsurface sedimentary information from beach ridges and other geomorphic landforms (Neal et al., 2003; Maurya et al., 2005; 2006; Sridhar and Patidar, 2005; Deshraj et al., 2012). The use of this method is continuously increasing in many fields including geomorphology, sedimentology, geophysics, archaeology, civil engineering, and remote sensing to solve many problems. However, in modern beach ridges, GPR mapping may have a problem with saltwater intrusion because it prevents radar waves to penetrate.

In continuation of the above discussion, it is also important to establish the chronology of such landforms (Nielsen et al., 2006; Clemmensen et al., 2012). The selection of the dating method is one of the decisive factors to construct the precise relative sea-level curve (Nielsen et al., 2017). Many studies have been done to know the exact chronology of the progradation of the beach ridges employing the radiocarbon dating method (Gupta, 1972; Agrawal and Guzder, 1972; McSaveney et al., 2006; Bird et al., 2007; Ribolini et al., 2011; Tamura, 2012; Lindhorst and Schutter, 2014; Shah-Hosseini et al., 2018). However, this method is only applicable to adequate amount of organic matter and has a problem of measuring the actual ages of marine shell samples due to the effect of marine reservoir (Choi et al., 2014; Souza et al., 2021). On the contrary, the OSL dating method uses sand grains (quartz or feldspars) produced by constructive waves having no drawback (except the areas where dim quartz exists) for dating and has been successfully applied in many studies (Choi et al., 2014; Remillard et al., 2015; Souza et al., 2021).

The combination of three different modern tools, namely high-resolution remote sensing, geophysical and geochronology datasets, is efficient in providing high-resolution past sea-level records (Dougherty et al., 2019). In the present day, these techniques have replaced traditional methods to obtain detailed past sea-level information (Tamura, 2012; Dougherty et al., 2019). In some of the studies, with the combination of the GPR technique and quartz optical dating, researchers have reconstructed the changes in Holocene sea-level (Dougherty and Dickson, 2012;

Clemmensen et al., 2012; Dougherty, 2014; Hede et al., 2015; Costas et al., 2016; Brooke et al., 2019; Barboza et al., 2021). In India, several attempts have been made with the same purpose using the methods of pollen, phytolith and coral (Banerjee, 2000; Kumaran et al., 2004; Banerji et al.,

2015), geomorphology (Pant and Juyal, 1993; Juyal et al., 1995; Loveson et al., 2001; Kunte and Wagle, 2005), geochemistry (Sharma et al., 2021; Dabhi et al., 2021), radiocarbon and OSL dating (Nair, 1974; Hashimi et al., 1995; Alappat et al., 2015; Loveson and Nigam, 2019). Gupta, (1972) established the chronology of elevated beaches and inland coral reefs along the Saurashtra coast, Western India. This study revealed that the sea-level was 1 to 3 m above the present monsoon high tide level during 5550 ± 1000 B.P. On the other side, the results from the study of Agrawal and Guder, (1972) show that sea-level was at -3 to 6 m in the central west coast of India. This variation may be because of the fact that elevation has been considered from the tidal level rather than from the mean sea-level (MSL). The Holocene sea-level of the western continental shelf of India was reconstructed from different sediment cores and found that the sea-level was -92 to -55 m during 10000 years BP (Nair, 1974). On the west coast of India, Hashimi et al. (1995) prepared a Holocene sea-level curve using several radiocarbon dates. This curve shows that the sea-level was more or less stable in the last 7 ka. Approximately 18,000 years ago, during the last glacial maximum, sea level was about 100-120 m below the present sea-level and afterward sea-level kept rising except slight fluctuations until around 7,000 years ago. There are some studies that deal with the reconstruction of the regional relative sea-level on the west coast of India (Alappat et al., 2015; Sharma et al., 2021), have reported that higher (high stand) sea-level existed during the Early to Mid-Holocene and followed by series of regressions. Most of this research was based on the mean tidal water level rather than the mean sea-level.

From the above studies, it is observed that the evolution of Holocene beach ridges on the west coast of India is not well documented in the literature so far. There is no study regarding the application of GPR to the problem at hand has been reported so far. For this, together with GPR and OSL dating methods, the present study aims to explain the evolution of beach ridges and changes in the Holocene relative sea-level on the central west coast of India.

2. Regional setting

The study has been carried out at Malvan beach, located on the central west coast of India. Here beach ridge system runs parallel to the present coastline and extends 1 km towards the landside with wide plain (Fig. 1). The sequence of ridges and swales produces topographic high and low ranging from 1 to 5 m with respect to mean sea-level and altitude of ridges is gradually increasing away from the sea. The surrounding region of the study site consisting of plateau and plain, represents a rugged topography. The area is bounded by two major rivers namely Gad in the northern part and Karli in the southern part supplying sediment flux on this coast. The tidal range of the Malvan coast is between ~0.1 and ~2.5 m. The area experiences mixed semi-diurnal tide with two high and two low. The wind direction is not consistent throughout the year. Though, the average speed of wind is 15.8 km/h, it reaches around 20 km/h during the southwest (summer) monsoon season.

Geologically, most of the area is developed on a basement of basalt flows of the Deccan volcanic province. The Proterozoic formations include the Kaladgi group (sedimentary rock types) which comprises conglomerate, sandstone, and shales and the recent Pleistocene formation contains soil, alluvium, laterite and sand deposits (Kumaran et al., 2004; Hanamgond and Mitra, 2008). The central west coast of India was tectonically active during the Mio-Pliocene Epoch and the coastal block faulting and uplift of the Western Ghats left an enduring effect of the neotectonics in the coastal tract, resulting in the development of several major lineaments (Tandale, 1993; Deshpande, 1998). Lineaments of the study area have been identified by Hanamgond and Mitra, (2008); Prasad et al., (2020) (Fig. 1d). The orientations of these lineaments are almost in NE-SW directions and a major lineament runs parallel to the coastline. These lineaments play a key role in the physical settings of this coastal sector (Powar, 1993; Biswal et al., 2003, Hanamgond and Mitra, 2008). According to Powar, (1993) the alongside of the Western Ghats and lineament patterns are indicative of vertical uplift. Geomorphologically, the area possesses a diverse combination of geomorphic features such as beach ridge and swale, spit, floodplains, tidal flat, backwater lagoon, wave-cut platform, cusped foreland, island, estuary, creek, and bar systems that make it distinct from the rest of Indian coast (Hanamgond and Mitra, 2008). The existence of beach ridges, coral reefs, and lignite beds with in situ mangroves high above the present msl along the central west coast of India has manifested the evidence of both submergence and emergence coasts (Sukhtankar and Pandian, 1990; Powar, 1993; Kumaran et al., 2004). The ridges are made up of fine to medium sand materials and are covered with vegetation whereas swales are composed of fine-grained peat soil and are devoid of vegetation cover. The research area comes under a sub-tropical climate with an annual mean rainfall around 2275 mm (Prasad et al., 2020).

Materials and methods

To achieve the aim of the current research, InSAR, beach topography measurement, GPR survey, texture analysis and OSL dating have been done.

2.1 Interferometry synthetic aperture radar (InSAR) data

The InSAR technique has ability to map the ground deformation resulting from tectonic activity (Burgmann et al., 2000; Argyriou et al., 2016; Lakhote et al., 2021). In the previous studies (Chen and Liu, 2000; Abelson et al., 2003; Hu et al., 2006; Mazzotti et al., 2006; Huang et al., 2006;

Čyžienė et al., 2007; Ramos et al., 2010), the neotectonic deformation has been measured applying InSAR and Persistent Scatterers-InSAR (PS-InSAR). In the present research, the advantage of InSAR has been utilized to understand the deformation in the central west coast of India and adjoining Western Ghats.

In this study, Sentinel-1 single look complex (SLC) products in IW mode were obtained from the European Space Agency (ESA) on the dates of 09.03.2017 and 29.03.2020. These datasets have been processed in SNAP software. The area of interest has been carved out from the IW mode of images to increase the processing speed. For the orbit file correction and coregistration of the images, apply orbit file and back geocoding have been used, respectively. An interferogram has been generated from the phase difference of the master and slave images. TOPS deburst has been applied to join the burst datasets into a single image. Topographic phase removal and range doppler terrain correction of the images have been performed using SRTM DEM (30 m resolution). For the purpose of filtering the phase band, goldstein phase filtering has been employed. Phase unwrapping and phase displacement have been done for the final displacement map. The flow diagram of InSAR data processing is given in figure 2.

2.2 Coastal topography and benchmark

The beach ridges and swales of the study region and its topographic highs and lows are quantified from the very high-resolution Cartosat (1.1 m), LISS IV (5.8 m) and field survey. High resolution differential global positioning system (DGPS) survey has been conducted along the GPR profiles at an interval of 5 to 30 m, with a vertical accuracy of 0.3 m. The benchmark for the present mean sea-level of the study site has been established using the datasets of the National Hydrographic Office (<https://hydrobharat.gov.in/>) and the Survey of India (<https://www.surveyofindia.gov.in/>). The berm and boundary of the beach and dune have been identified from the high-resolution continuous images and beach profiling. The profile drawn across this ridge and swale topography of the study site is

almost continuous up to the R-2. Thereafter this continuity was broken since the GPR instrument had to be moved around 130 m in the south-east direction for the presence of water in S-3 (Fig. 1e).

2.3 Ground penetrating radar (GPR)

A 200 MHz (central frequency) GPR antenna (SIR 4000) developed by GSSI (Geo-physical Survey System Inc.) has been used to acquire the GPR profiles. The survey was conducted in the winter season (February, 2019 and March, 2020) to avoid the rise of water level in the summer monsoon season. Along the ridge and swale topography, GPR data was acquired from the landside to the present shoreline (Fig. 1e). Topographical data has been integrated with the GPR profiles to obtain the actual depth of the subsurface image. The penetration depth of the radar waves was 6 m (120 ns). Few parameters such as sample/scan 512; bits/sample 32; unit/mark (m); scans/unit (m); scans/s 50; dielectric constant 7; high pass 30 (MHz); low pass 500 (MHz); gain range (-5), (41), (57), (57), (59) were tuned in header file based on field condition before the commencement of the survey. Besides, the survey wheel was calibrated with the field distance during the survey. Garmin GPS was used to obtain the geolocation of the radar image. At first, repeated reflection data were recorded along a particular profile to verify the consistency of data.

The acquired data was processed in Radan 7 (developed by GSSI) and MatGPR 3.2 (compatible with Matlab) software. The depth (m) of the radar profile has been derived from the reflected 230 signals in two-way travel time (TWT). The depths from the homogeneous and isotropic materials have been measured by the equation $d = \frac{v_r \cdot t}{2}$ where v_r (relative propagation of velocity) calculated from $\frac{c}{\sqrt{\epsilon_r}}$ here ϵ_r represents relative permeability and t defines the TWT from the $\sqrt{\epsilon_r}$ target (Daniels, 2004). The air gap between the transmitter and receiver of the GPR profile has been vertically adjusted to get the accurate depth using time zero correction (GSSI, 2015; Prasad et al., 2023). Horizontal background removal has been done to eliminate the noise of similar reflections that appeared in the image. To remove the insignificant noise of the raw data, boxer filter has been applied in high pass (30 MHz) and low pass (500 MHz) frequency (GSSI, 2015; Prasad and Loveson, 2020). The mean, median, exponential, and power decay attenuation curves 23 of each of beach ridge and swale have been generated from the MatGPR software to get the sub surface information of radar wave attenuation (Tzanis, 2010). Velocity spectra is one of the velocity measurement methods which estimates velocity using cross-correlation method (Neal, 2004; Loveson et al., 2014a; Prasad and Loveson, 2020). In this method, inversion of reflection amplitudes has been employed to measure the reflection coefficients for calculating the velocity of sedimentary layers (Forte et al., 2014).

3.4 Textural analysis

A total of 23 samples (17 samples from 4 beach ridges and 6 samples from 2 swales) was analysed for deriving information about the textural parameter, specifically about sand-size fraction. Approximately ~120 grams of each sample were weighed carefully and soaked in the distilled water for dispersion. After separating the lumps, these were filled with 1000 millimeters (ml) distilled water and kept overnight to make samples salt-free. The salts from the samples were removed by repeated washing with distilled water, and excess water was removed by decanting tube. After that, 10 ml of 10% Sodium hexametaphosphate was added to the sample in a beaker. The sample containing Sodium hexametaphosphate was being stirred at an interval of 20 minutes and this process was repeated for up to 4 hours. Subsequently, carbonates and organic matter were extracted by treating them with Hydrochloric acid (HCl) and Hydrogen Peroxide (H₂O₂).

Approximately ~100 grams of each sample were taken for the analysis. The grain size has been obtained using a mechanical sieve shaker consisting of 6 sieves of 63 micrometer (μm), 125 μm , 250 μm , 500 μm , 1000 μm and 2000 μm . All the fractions (range) were weighed cautiously, and the percentage of every fraction was measured for each sample. Sand fraction varies from $>63 \mu\text{m}$ to 2000 μm (very fine sand = 63-125 μm , fine sand = 125-250 μm , medium sand = 250-500 μm , coarse sand = 500-1000 μm whereas very coarse sand = 1000-2000 μm). The grain size $>2000 \mu\text{m}$ represents gravel, and $<63 \mu\text{m}$ grain size shows a mixture of silt and clay grain size.

For clay particle size analysis, the remaining ~15 grams out of 20 grams of each sediment sample were taken. Sand, silt, and relative clay ratios were measured following the standard sieving and pipette method (Carver, 1971; Folk, 1980). Of the total amount of sample, 63 μm particles were taken into account for the wet sieving. The washing was continued until the clear water passed through the sieve. Care was taken to show that the total amount of water below the 63 μm does not exceed 1000 ml. The coarse fraction obtained in the sieve was dried and weighed, representing the sand fraction's total weight ($>63 \mu\text{m}$). The mud fraction of $<63 \mu\text{m}$ size (clay+ silt) collected in a 1000 ml glass cylinder was subjected to pipette analysis for estimation of clay fraction and silt as per the procedure given by Folk, (1980).

3.5 Optically stimulated luminescence (OSL)

The optically stimulated luminescence dating method utilizes the radiation dosimetric properties of mineral grains. The beach ridges of the study area have a sufficient amount of quartz material which is suitable for OSL dating. A total of ten samples (below the surface deposit) along the GPR track were collected in opaque plastic tubes (length ~25 cm and inner diameter ~5 cm) for dating. Out of these,

three samples were taken from each beach ridge (except ridge 4) at depths of 2, 1.5, and 1 m. Due to the presence of water table in ridge 4, only one sample was collected at 0.8 m depth. These samples were processed in subdued red-light conditions. The outer 2 to 2.5 cm of the sample from both ends of the tube is kept for dose rate determination and in-situ water content measurement while the remaining sample was chemically treated to extract quartz for estimation of equivalent dose (De). Standard sample processing protocol was used as described by Aitken, (1998). The samples were treated with 10% HCl for 12 hrs followed by treatment with 30% H₂O₂ to remove the carbonates and organic impurities, respectively. Then, dried samples were sieved to get sand grains in size fraction of 90-150 µm. From this, quartz grains are separated using Frantz Magnetic separator at two different magnetic fields generated by passing 0.5 A and 1.5 A currents (Porat, 2006). The grains were then etched with 40% hydrofluoric acid (HF) for 60 minutes to remove the alpha skin and residual feldspars, if any. The HF-treated samples were immersed in

37% HCl to convert insoluble fluorides to soluble chlorides. The obtained quartz grains were sieved to get the desired grain size range and were tested for their purity using infrared stimulated luminescence (IRSL) response for three representative aliquots. IRSL test was conducted to check the feldspar contamination in the quartz grains. The absence of luminescence signal confirmed the purity of the quartz sample. There was no response observed to IR stimulation. Saturated water content of the samples was measured using the following formula:

$$\text{Water content (\%)} = (\text{Saturated weight} - \text{dry weight}) / (\text{Sample weight})$$

Each sample with 24 aliquots was prepared by spreading about 100-200 quartz grains over 3 mm on 9.8 mm stainless steel discs using silicon spray. Blue light was used to stimulate the quartz aliquots and hence the process is also called Blue Light Stimulated Luminescence (BLSL). For

BLSL measurement, a Risoe TL/OSL reader (DA-20) system was used (Bøtter-Jensen et al., 2000). Blue light stimulation (BLSL/OSL) comprised of blue light LEDs emitting at 470 ± 30 nm, and IRSL was measured by stimulating with IR LEDs emitting at 870 ± 40 nm (Bøtter-Jensen et al., 2000). Typically, 70% of the full power of LED (delivering an estimated 50 mW/cm² blue light at the sample) was used for stimulation. The detection optics comprised a 7 mm Hoya U-340 Blter allowing a transmission band of 290–370 nm with a peak at *340 nm.

Single aliquot regenerative dose (SAR) technique of Murray and Wintle (2000) was used to measure De. The estimated De values were accepted if the following criteria were achieved (i) recycling ratio within 10% of the unity, (ii) error to be less than 20%, and (iii) recuperation (ratio of luminescence signal of zero dose to that of the natural) signal below 5% of computed De value. The central Age

model was used to compute De from the set of data of each aliquot. For radioactivity, the concentrations of uranium (U), thorium (Th), and potassium (K) of each sample were calculated using high-purity Germanium crystal (HPGe) gamma-ray detector. This procedure was done by comparing the well-identified gamma rays from the sample and standard radioactive concentrations. Dose rate and OSL age have been calculated using dose rate and age calculator (DRAC) software (Durcan et al., 2015).

4. Results

4.1 Regional tectonic and beach morphology

The present deformation map of the central west coast of India has been prepared using the InSAR method (Fig. 3). This map covers the study site and its south and eastern portions. The results exhibit that uplifting and subsidence are taking place with an average rate of 2.5 mm/yr and 1 mm/yr, respectively. The map reveals that most of the Western Ghats region is experiencing upliftment, while the coastal sectors range from stable to subsidence. Various factors cause upliftment and subsidence, including tectonic effects, fault displacement, human activity, and earthquakes. In the present time, the subsidence of coastal zones and cities in South, Southeast, and East Asia is primarily caused by human activities especially groundwater extraction, as reported by Wu et al. (2022).

By the definition of beach ridge, it is observed from the images that the shape of beach ridges of the study region is parallel to the coastline which is the first indication of the past sea-level changes (Fig. 1). A total of four ridges (three paleo beach ridges and one modern beach ridge) and contiguous swales have been recognized as the topographic highs and lows, respectively from the high-resolution satellite images and field surveys. Swales separating the beach ridges are topographically flat plain which frequently gets waterlogged (water depth ranges between 10 and 60 cm). Plant materials grown in soil, in due course of time have transformed into organic soil on the surface. In general, the dimension of the beach ridges is directly related to the sediment influx.

In this study, the dimensions (in width) of the ridge-1 (R-1), ridge-2 (R-2), ridge-3 (R-3), and ridge-4 (R-4) are 288 m, 93 m, 152 m, and 160 m, respectively whereas the swale-1 (S-1), swale-2 (S-2), swale-3 (S-3), swale-4 (S-4) are of 165 m, 90 m, 28 m, and 107 m, in expanse respectively

(Fig. 4). The current beach profile of the study area is depicted in figure 4b along with field photos. This profile displays the elevations of the beach-dune contact (0.75) and the berm (0.45), which have been utilized in modern analogs.

4.2 Stratigraphy

The interpretation of the GPR sub-surface images is based on the principles of radar facies and radar surfaces which are briefly discussed by Neal, (2004); Clemmensen and Nielsen, (2010); Lindhorst and Schutter, (2014). On the basis of the reflection, velocity and attenuation of the radar waves, the GPR image has been classified into three radar facies as Rf1, Rf2, and Rf3. Rf1 indicates the ground surface and uppermost deposit with variable thickness. The reflectivity of this facies is sub-parallel to seaward dipping with low to moderate amplitude, mainly explained as aeolian and dune ridge deposits. Rf2 is the middle layer below 1-2 m and consists of moderate to high amplitude radar waves with high seaward dipping which define the beachface deposit. Although, a few flat and landward reflections are also observed in this layer. Rf3 is the lowermost sedimentary deposit with weaker and less continuous in increasing depth due to the spreading and loss of the signal. The radar facies of this layer are flat to low seaward dipping which is characterized by shoreface deposition. These layers are very common in beach ridges which are also observed in other studies (Dougherty, 2014; Hede et al., 2015). Two radar surfaces have been identified in the beach ridges based on the pattern of radar facies and velocity of the radar waves

(Fig. 5). Radar surfaces of the beach ridges have been explained by Clemmensen and Nielsen, (2010) and Lindhorst and Schutter, (2014). On the other hand, multiple horizontal and parallel positive and negative couplets just beneath the surface have been detected from the GPR profiles of swales (Fig. 6). Additionally, many diffraction hyperbolae have been observed in the radar images. These hyperbolae can be found in the images of beach ridges mainly due to the presence of buried boulders or voids in sediments. They can also be generated from objects above the ground surface for example trees or fences (Jol, 2008). In the present study, diffraction hyperbolae (Fig. 5, 6, 7) are likely caused by roots in the beach ridge area. For the buried objects, the migration process can be followed for better comprehension of the velocity of radar waves. Otherwise, differential hyperbola will over-migrate and produce U-shaped smiles leading to misinterpretation. For this valid reason, migration is not applied in the present research. These hyperbolas have also been recognized in other beach ridge studies (Lindhorst and Schutter, 2014; Gouramanis et al., 2020).

Attenuation curves have been prepared to understand the attenuation of radar waves in ridges and swales. These curves include mean attenuation, median attenuation, exponential decay and power decay. In these curves, instantaneous power (y-axis) has been plotted against the TWT in ns (x-axis). It can be seen that the mean attenuation of R-1 and R-2 is around 10^{14} and the same for R-3 is a bit more

than 10^{13} . On the other side, the mean attenuation of S-1, S-2, and S-3 is comparatively lesser (around or less than 10^{13}) than the neighbouring ridges due to the presence of water content and mudflat. This study points out that the ridges are less attenuated up to 80 ns whereas in the case of swales attenuation starts going up after 50 ns (Fig. 8).

In the velocity diagram (Fig. 9), the y-axis expresses the velocity of the radar wave with respect to two-way travel time (TWT) in the x-axis. In general, a high amplitude zone in radar data represents strong dielectric contrast between the sediment deposits interpreted as heterogeneous lithology and vice versa (Shan et al., 2016). The maximum velocity has been observed in the ridges (R1, R2, and R3), owing to different stratigraphic layers. In regards to the swales (S1, S2, and S4), mix velocity variation has been recorded because of existing water and mudflat which obstructed the radar waves in the top surface.

4.3 Sedimentology

The grain size results of the ridge and swale are described in Table 1. In the R-1, the average share of 125-250 μm and 250-500 μm grain size classes are 63.7% and 30.1%, respectively and the remaining portion (6.2%) belongs to the other classes. Regarding R-2, the mean grain size in the

125-250 μm class is 48.2% followed by 46.3% (250-500 μm), 4.4% (63-125 μm), 0.9% (<63 μm).

In the case of R-3 and R-4, 86.39% and 77.37% of the total mean grain size are included in the 125-250 μm class, respectively. On the other hand, in S-1, the maximum portion of average grain size comes under the class 125-250 μm (49.68%) followed by 250-500 μm (32.68%), <63 μm (7.36%), 63-125 μm (5.48%). The grain size distribution of S-2 quite resembles the pattern of S1. It is noticeable that the grain size percentage of <63 μm has increased with depth in both S-1 and S-2. Overall, this analysis demonstrates that a larger share of grain size falls into the classes of fine sand to moderate sand which are moderately well sorted to well sorted. Similar results have been found from the beach ridges of the southwest coast of India (Alappat et al., 2015).

4.4 Chronology

The results of quartz optical dating are summarized in Table 2. The ages of the samples as determined, indicate their occurrence in the Holocene. The OSL ages help understand the progradation of beach ridges. The three samples of the OSL (R1D2, R1D1.5, and R1D1) collected at different depths in R-1 reveal that this beach ridge was developed ~7.7-8.7 kyr. The age range of the samples from R-2 (R2D2, R2D1.5, and R2D1) lies between ~4.1-4.7 kyr. The samples' age of the third ridge (R3D2, R3D1.5, and R3D1) vary from 0.91-1.2 kyr which means this beach ridge is thousand years old. In the case of

the fourth ridge (R4D0.8), one sample has been dated with an estimated age of ~ 0.12 kyr suggesting that this ridge is of recent origin.

The amplitude and size of the ridges and swales are the indicators of the progradation of the beach ridges. Beach ridge progradation has been calculated from the distance divided by the difference of age between the beach ridges. The average progradation rates of the beach ridges are as follows:

0.12 m/yr from 7.7 ± 0.6 to 4.7 ± 0.3 kyr (R1D1.5 to R2D2), 0.03 m/yr from 4.7 ± 0.3 to 1.0 ± 0.05 kyr (R2D2 to R3D1), and 0.27 m/yr from 1.0 ± 0.05 kyr to 0.12 ± 0.01 kyr (R3D1 to R4D0.8) (Fig. 10). In this study, the average progradation rate as computed from the oldest beach ridge to the present beach ridge is 0.14 m/yr but has not been constant over the Holocene age. These progradation rates are measured on the basis of long-term averages that may vary from actual progradation. Even, this might have been punctuated by periods of coastal stability. The relative ages and errors of the SLIPs are calculated using the regression method as described in Barboza et al. (2021).

4.5 Relative sea-level construction

Two morphological features, namely berm and boundary of beach and dune have been used to measure the elevation of past sea-level. The measured elevations of the present beach-dune boundary and berm are 0.75 ± 0.10 m and 0.45 ± 0.15 m above msl, respectively. The error has been considered from the old and new beach profiles. It is also important to mention that the elevation and spatial displacement of the berm can change with seasonal climate variations and tides (Costas et al., 2016). Though, the present study site is relatively stable as observed from the previous images. Twenty-six toplap terminations of the radar images are represented as berm indicators while twenty-one downlap terminations illustrate the boundary between the dune and beach. To obtain precise elevation values of these points, it has been digitized in the Origin software. The extracted points are transformed into sea-level indicator points by subtracting the elevation of the modern berm and contact between the beach and dune from toplap and downlap points, respectively. The obtained elevations, ages and cross-shore distances have been correlated with each other to understand the past sea-level (Fig. 11). Fig. 11a shows the elevations of the beach-dune and berm sea-level indicators with distance from landward to seaward. From this figure, it can be seen that the sea-level initially rises in ridge 1 and is followed by the fall of sealevel from 2.5-3 m highstand which is also observed on the coasts of Brazil (Hein et al., 2014). The relative ages of the sea-level indicator points from both indicators have been calculated from the OSL ages and plotted with respect to the cross-shore distance (Fig. 11b). It is noticed from this figure that the linear relationships of the coefficient of determination are 0.92 and 0.95 for the beach-dune boundary and berm, respectively. To prepare the relative mean sea-level, the age and

elevation of the sea-level indicator points have been plotted (Fig. 11c). It is essential to consider the error in relative mean sea-level. The increasing depth of the GPR profile leads to greater heterogeneity of the sub-surface material and high attenuation, resulting in increased errors. As a consequence, the error of the GPR profile is more pronounced in Costas et al. (2016) compared to Barboza et al. (2021). However, since the depths of the GPR profile are less than 6 m in the present study, the maximum error for the 200 MHz frequency GPR is considered 0.30 m (Jol, 2008; Barboza et al., 2021). A total of 0.6 m and 0.65 m errors have been included in this research considering the GPR (0.3 m) and beach profile (0.3-0.35 m). The relative sea-level shows a variation from 2.3 to 1.2 m from the beach-dune indicator whereas it is 2 to 1.4 m from the berm indicator during the mid- to late-Holocene. This sea-level is almost identical to the sea-level curve of the west coast of India prepared by Hashimi et al. (1995). From these figures, it is observed that the berm indicator shows slightly better agreement compared to the dune-beach boundary which is also reflected in the study of Costas et al. (2016).

In figure 12, the sea-level data of the Indian coast from different studies have been organized with respect to the mid- to late-Holocene ages. It is evident from the figure that the past sea-level elevation predominantly ranged from 0.5 to 3.5 m and the trend of sea-level ranged from 2 to 1 m during the mid- to late-Holocene. The results of the present study also fall within this range. However, it is important to note that the sea-level of most of these previous works is based on the mean low tide level rather than the mean sea level. Recently, Sharma et al. (2021) have reconstructed the relative sea-level in the Gulf of Kachchh are 1.45 ± 0.33 m and 0.53 ± 0.33 m above msl during the mid-Holocene and late-Holocene, respectively.

5. Discussion

The long-term geomorphological evolution in the coastal region must be comprehended to evaluate and predict how shoreline dynamics is likely to get affected by sea-level changes, sediment dynamics and energy exposure (Loveson et al., 2014b; Sander et al., 2016). The current research aims to build a more robust chronological framework based on beach ridges for tracing shoreline migration during the Holocene age in the central west coast of India.

5.1 Ridge and swale as a sea-level indicator

Selecting the correct geomorphic indicator for paleo sea-level reconstruction in a specific coastal region is of vital importance. Many studies have considered both ridge and swale while some studies consider only ridge as a sea-level proxy based on the field conditions for example no or limited mud, dry topsoil, less saltwater intrusion, and limited aeolian cover. From the attenuation curve (Fig. 8), it is evident that the beach ridge is the best past sea-level marker compared to the swale because of less

attenuation and clear records of past sea-level. Moreover, the velocity diagrams (Fig. 9) of the ridges reveal that the velocity has reached its maxima in the contact zone of aeolian and beachface while swales have less velocity by reason of water content and mudflat. Clemmensen and Nielsen (2010) estimated that the difference in sea-level between ridge and swale is 1 m. Hence, beach ridge has been considered for sea-level proxy not swale due to the significant deflation resulting in lowering the structures after their formation. Taylor and Stone, (1996) have mentioned that the past records of the beach ridges remain well-preserved in the wider beach ridges. Moreover, it is worth mentioning that the long-term mean sea-level reflected by appropriate beach ridge systems. The coarse-grained beach ridge in the beach ridge systems formed by a single storm event does not represent the long-term average wave condition (Tanner, 1995; Billy et al., 2015). This heterogeneity in the beach ridge system is primarily influenced by the intensity of local processes such as fetch length, storm surge, and storm duration rather than the long-term elevation of relative sea-level. On the contrary, each paleo beach ridge of the present study region is the result of wave action which makes it suitable for reconstruction of relative sea-level changes with time.

5.2 Limits of paleo sea-level indicator

The reconstruction of past sea-level from the deposition of paleo beach ridges is well-known with different sea-level markers. Earlier, elevation of beach ridges has been considered as a marker of the paleo sea-level. However, with the march of time, it has been observed that this indicator is not appropriate as the deposition of aeolian sand creates uncertainty in establishing the relationship between the actual altitude of the ridge and sea-level. To address this issue, Bjørnsen et al. (2008) used an average value of 0.5 m to describe this deflation to define the sea-level, though this value cannot be uniformly applied to all beach ridges worldwide due to the heterogeneity of coastal configurations, geomorphological processes, and clast content in the beach ridge deposits (Nielsen and Clemmensen, 2009). Heteren and Plassche, (1997) have revealed that the boundary between dune and beach sediments is clearly identified from the GPR sub-surface image. Later, Heteren et al., (2000) concluded that this boundary produced a well-constrained past sea-level indicator.

Many researchers have used the same indicator for the reconstruction of past sea-level (Dougherty, 2014; Costas et al., 2016; Dillenburg et al., 2017; Oliver et al., 2020; Barboza et al., 2021). Considering this, in the present work, the boundary between dune and beach has been readily defined from beach ridge profiles based on the radar facies while it is not distinctly visible in the swale images, because of the high attenuation of radar waves.

5.3 Sedimentary architecture of beach ridge and swale

The sub-surface radar facies of beach ridges are not often similar throughout the world. Even, they differ within one beach ridge system of an area due to the varying rates of accumulation of sediment, wave height, and storm events during each beach ridge formation. However, they have some common characteristics such as seaward dipping of radar facies and boundary between two radar facies (radar surface) which have been observed in most of the paleo beach ridges (Nielsen and Clemmensen, 2009; Lindhorst and Schutter, 2014; Gouramanis et al., 2020). In the present study, sediment deposits have many differential hyperbolas which act as an obstacle to see the radar facies. Despite this, many dipping patterns with low to high amplitudes have been identified. It is important to identify the termination patterns (boundaries) for the construction of a relative chronology since this is representative of chronostratigraphic gaps. Laws of superposition and cross-cutting relations can be used to determine the relative chronology of successive radar data. Considering that, radar stratigraphy often distinguishes between two distinct radar facies differentiating termination patterns and reflections (Neal et al., 2003; Shan et al., 2016). In this study, R-1, R-2, and R-3 profiles of the GPR show that the radar facies have mainly westward

(seaward) dipping (Fig. 5), implying regression formed by wave action. However, a few eastward (landward) dipping which has been also observed in the profiles, indicates the activity of washover processes (Clemmensen and Nielsen, 2010). It can be inferred from the limited amount of wash-over deposits that waves rarely flooded the beach ridges in this environment. The presence of thick mud in the swale is the probable reason where electromagnetic waves have bounced within sedimentary units and overprinted any stratigraphy (Gouramanis et al., 2020). However, there are some seaward dipping radar facies that have also been seen in swales. Besides these paleo beach ridges and swales, the present beach ridge shows both landward and seaward radar facies which indicate that probably wash-over deposits have resulted from storms or high waves. It can be stated that in the present time these events have got intensified on this coast. However, due to the lower elevation and saltwater intrusion, the high attenuation of the radar signal has limited the availability of detailed information (Fig. 7). As a result, SLIPs have not been identified in ridge 4. Several previous studies (Costas et al., 2016; Barboza et al., 2021) have correlated SLIPs with the current beach profile (berm and beach profile) to accurately estimate past sea levels. For this reason, the present study has also correlated berm and dune-beach markers with the SLIPs.

5.4 Beach ridge and swale formation

The main process responsible for the formation of beach ridges around the world includes fairweather waves along with aeolian foredune accumulation in prograded sandy beach ridges and storm waves building the gravel ridges (Tamura, 2012). Predominantly, the sandy beach ridges are seaward dipping stratification due to swash and backwash processes whereas gravel beaches are mainly landward dipping due to storm waves. In the current research, seaward dipping is associated with the fair-weather waves process for beach ridge formation. In contrast, in the study of Psuty (1965, 1967), it was observed that the landward dipping of sandy beach ridge was attributed to storm waves. The deposition of sand in fair-weather waves is not the only statement that supports the origin of ridge and swale topography. These waves can generate a broad flat aggradation surface rather than the sequence of beach ridge and swale. In general, beach ridges cannot exist without swales except for a single broad platform (Tanner, 1995). Noticeably, many studies have addressed the formation of beach ridges but not the swale formation. There are many arguments for the separation of beach ridges in several studies (Tanner, 1995; Taylor and Stone, 1996; Goy et al., 2003; Kelsey, 2015). After reviewing these articles, it can be stated that the beach ridges are isolated by storms, by sediment supply due to climate change, or by sea-level change. These factors can interact and reinforce one another, ultimately leading to the isolation of a beach ridge. Among these factors, the beach ridges are mostly found under the situation of regression (BjoØrnsen et al., 2008; Tamura et al., 2012; Clemmensen and Nielsen, 2010) where progradation is mainly driven by falling relative sea-level. On the other side, a few beach ridges are formed by high sedimentation rates where the relative sea-level is stable or rising (Forbes, 1994; Billy et al., 2015). From the result of sea-level (Fig. 11a,b,c), it can be stated that the evolution of present beach ridges is mainly the result of falling relative sea-level. However, the rate of sea-level falling is not the same during the mid- to late-Holocene. The minor fluctuations in sea-level make the energy level of waves different (Tanner, 1995). After 7200 BP, Loveson and Nigam (2019) reported five minor sea-level fluctuations on the east coast of India while Bhattacharya, 2021 showed two events of high relative sea-level on the east of coast India. The small sea-level rise in a certain period increases the high energy of wave action in the surf zone due to the less energy take off as the new high-water level achieves. Therefore, the run-up of the swash is increased resulting in the deposition of sand. The drop in sea-level from the previous position reduced the run-up of the wave energy. As a result, the deposition of sand during the higher position of sealevel generates a beach ridge and the deposition of new sand during the falling of sea-level produces a swale. For this, the heights of ridge and swale vary with each other. In the study of Clemmensen and Nielsen, (2010), it was seen that most of the swash build beach ridges are 0.2 to 0.6 m higher than the adjoining swales except only a few ridges are 1 m

or higher than the adjacent swales. Subsequently, in the present work, the elevation range of ridge and swale is 0.5 to 1.2 m (Fig. 4). Tanner, (1995) discussed different processes of the origin of beach ridges and swales and concluded that the small sea-level fluctuation is the major reason for their formation. On the contrary, Dougherty, (2014) showed the storm-initiated beach ridge and swale formation in Omaha, New Zealand. As such, the genesis of beach ridges and swales in any given region is largely contingent upon both global and local processes. The schematic diagram displays the evolution of beach ridges and swales with reference to sea-level (Fig. 13).

The frequency and size of ridge and swale primarily depend on the number and duration of sea level fluctuations. The minor fluctuation of sea-level is reflected in the frequency of beach ridge and swale. Therefore, the number of beach ridges on the west coast of India is less compared to the east coast of India. Goy et al., (2003) demonstrated that the size of the ridges and swales changes and even reverts. The higher rate of sediment accumulation gives rise to smaller beach ridges and vice versa. In the present study, the beach ridges are not homogenous due to different rates of sediment accumulation and the main source of this accumulation is from offshore. On the other hand, the elevation of the ridge and swale relies on the magnitude of sea-level changes. Bhattacharya et al., (1979) studied the beach ridges of the southwest coast of India and concluded that the slightly higher elevation of the older beach ridge as compared to the younger beach ridge is evidence of hiatus in progradation.

5.5 Causes of sea-level fluctuation

There are multiple processes including eustasy, isostasy, hydro and glacio isostasy together with local to regional tectonic (upliftment and subsidence), variation in oceanographic and atmospheric circulation responsible for the relative sea-level changes (Milne et al., 2009). As a result, the rate of sea-level changes in different regions of the Indian coast is not uniform. The relative sea-level curve constructed for the east coast of India for the Late Pleistocene and Holocene Period (Loveson and Nigam, 2019) discussed various stages of sea-level changes between 15000 BP to Recent. Another few studies (Loveson, 1994; Loveson et al., 1996) indicate regional coastal uplifts along the east coast which could be corroborated by the sea level fluctuations. However, the sea level fluctuations were slightly different along the west coast of India as evidenced by the existing geomorphic setup. Hashimi et al. (1995) observed that during 14,500 BP, the sea level was ~100 m depth and rose to 80 m depth during 12,000 BP (~10m/1000yr) and between 10,000 to 7,000 B.P, the rate of rise was comparatively higher (~20m/1000yr). During this transgressive period, the rate of sea-level rise was ~ 1 cm/per year until 6000 years ago. This sea-level was ~2 m above the present, as shown by the present and other studies (Fig. 12). The switch from the transgressive phase to the regressive phase was near-coincident with the well-documented decrease in the rate of sea-level rise from 6000 to 7000 years ago (Fairbanks,

1989; Subrahmanya, 1996; Fleming et al., 1998) which is also seen in the current research (Fig. 11). The cause of transgression and regression along the west coast of India is debatable because of scanty and unevenly distributed data. Subrahmanya (1996, 1998) discussed the several stages of tectonic, eustatic and isostatic movements of the west coast of India and concluded that the west coast of India had very little subsidence or upliftment during the Quaternary. Verma and Mathur (1979) proposed that the change in sea-level on the west coast of India is mainly of eustatic origin. On the other side, in the northern part of the west coast of India, tectonic plays a role in relative sea-level changes (Sharma et al., 2021; Banerji et al., 2015). Furthermore, other studies (Bruckner, 1989; Nair, 1974; Kale and Rajaguru, 1985; Wagle, 1994) indicated sea-level fluctuations along the west coast region based on raised beaches and terraces. All these studies have led the sea-level research to further fathom towards the future understanding of tectonics contributions. The finding from the present deformation map may demonstrate neotectonic effects in this region which are also evident on the southwest coast of India (Alappat et al., 2015). In future research, a deformation map of the study area can be prepared using the PS-InSAR method to exemplify the evidence of neotectonics with better precision. From the present research, it can be stated that the sea-level change during the mid-late Holocene is mainly the cause of a combination of tectonic and eustatic origin. Mann et al. (2019) also disclosed that the Holocene relative sea level changes in the Indian ocean were mainly influenced by global and local drivers. At this juncture, the present study is a contribution to the regional sea-level research in this region and would support the construction of a relative sea-level curve for the entire west coast of India.

5.6 Limitation and future scopes

The present study has reconstructed the Holocene relative sea-level using high-resolution GPR images and OSL ages. However, there are some limitations, including the core data of sediment, which needs to be correlated with the GPR sub-surface image and more sea-level indicator points could not be identified due to the field obstruction. Moreover, in the future, the applied modern tools and more advanced numerical models can be employed to determine the possibly multiple driving mechanisms for the observed changes and to prepare India's high-resolution sea-level curve from the thirteen beach ridges of India identified by Kunte and Wagle, (2005).

6. Conclusion

The beach ridges and associated swale deposits of Malvan beach, central west coast of India record the Holocene sea-level variation. The sedimentary architecture of these landforms has been deduced from GPR subsurface profiles and surface topography measured by automatic level instrument. As observed

in the field investigation, the sequential topographic highs and lows indicate ridges and swales, respectively. The morphological features, namely the berm and beachdune contact have been extracted from the geophysical survey and transformed into the sea-level marker. Three different layers including aeolian, beachface and shoreface deposits with parallel to seaward dipping radar facies in beach ridges have been demarcated. On the other side, multiple horizontal and parallel positive and negative couplets in the swale have been noticed because of the presence of mud. These beach ridges and adjoining swales are formed by sea-level fluctuation in fair-weather conditions. The transition of the Holocene transgressive and regressive record began around 7000 years ago when the sea-level was +2 m above msl. The average progradation rate of the beach ridges is 0.14 m/yr. The mid-late Holocene sea-level change is most likely due to the combination of tectonic and eustatic origins. Reconstruction of the internal architectural pattern of ridge and swale topography by GPR technique will be useful to further prepare the Holocene sea-level curve of India.

Acknowledgement

We acknowledge the support from the University Grant Commission (3160 NET-June 2015) to the first author. The authors are thankful to the Director CSIR-NIO for encouragement. We are also thankful to the Director of the Physical Research Laboratory for permitting us to use the laboratories. The authors are grateful to the reviewers for their critical comments and constructive suggestions to improve the manuscript. We extend special thanks to Prof. Amy J. Dougherty from the University of New South Wales, Sydney, for her excellent review of our manuscript. Field support from the survey team members is thankfully acknowledged. The NIO contribution number is.....

Credit authorship:

P Prasad: Conceptualization, Methodology, Field data collection, Investigation, data analysis & Writing the original draft. **VJ Loveson:** Overall supervision on the investigation, Review & editing. **V Kumar:** OSL dating and analysis, Review & editing. **AD Shukla:** OSL dating and analysis, Review & editing. **P Chandra:** Formal analysis, Interpretation, Review and editing. **S Verma:** Review and editing, **R Yadav:** Field data collection, Sediment sample processing and analysis, Review and editing **R Magotra:** Data analysis and interpretation, **GM Tirodkar:** Field data collection, Topography data analysis.

References

- Abelson, M., Baer, G., Shtivelman, V., Wachs, D., Raz, E., Crouvi, O., Kurzon, I. and Yechieli, Y., 2003. Collapse-sinkholes and radar interferometry reveal neotectonics concealed within the Dead Sea basin. *Geophysical Research Letters*, 30(10). <https://doi.org/10.1029/2003GL017103>
- Agrawal, D.P. and Guzder, S.J., 1972. Quaternary studies on the Western coast of India: Preliminary observations.

- Alappat, L., Frechen, M., Kumar, S.S., Babu, D.S., Ravur, R. and Tsukamoto, S., 2015. Evidence of Late Holocene shoreline progradation in the coast of Kerala, South India obtained from OSL dating of palaeo-beach ridges. *Geomorphology*, 245, 73-86. <https://doi.org/10.1016/j.geomorph.2015.05.006>
- Aitken, M.J., 1998. Introduction to optical dating: the dating of Quaternary sediments by the use of photon-stimulated luminescence. Clarendon Press, New York.
- Al-Mikhlaifi, A.S., Hibbert, F.D., Edwards, L.R. and Cheng, H., 2021. Holocene relative sea-level changes and coastal evolution along the coastlines of Kamaran Island and As-Salif Peninsula, Yemen, southern Red Sea. *Quaternary Science Reviews*, 252, 106719. <https://doi.org/10.1016/j.quascirev.2020.106719>
- Argyriou, A.V., Teeuw, R.M., Rust, D. and Sarris, A., 2016. GIS multi-criteria decision analysis for assessment and mapping of neotectonic landscape deformation: A case study from Crete. *Geomorphology*, 253, 262-274. <https://doi.org/10.1016/j.geomorph.2015.10.018>
- Banerjee, P.K., 2000. Holocene and Late Pleistocene relative sea level fluctuations along the east coast of India. *Marine Geology*, 167(3-4), 243-260. [https://doi.org/10.1016/S0025-3227\(00\)00028-1](https://doi.org/10.1016/S0025-3227(00)00028-1)
- Banerji, U.S., Pandey, S., Bhushan, R. and Juyal, N., 2015. Mid-Holocene climate and land-sea interaction along the southern coast of Saurashtra, western India. *Journal of Asian Earth Sciences*, 111, 428-439. <https://doi.org/10.1016/j.jseaes.2015.06.021>
- Barboza, E.G., Dillenburg, S.R., do Nascimento Ritter, M., Angulo, R.J., da Silva, A.B., da Camara Rosa, M.L.C., Caron, F. and de Souza, M.C., 2021. Holocene sea-level changes in southern Brazil based on high-resolution radar stratigraphy. *Geosciences*, 11(8), 326. <https://doi.org/10.3390/geosciences11080326>
- Bird, M.I., Fifield, L.K., I, T.S., Chang, C.H., Shirlaw, N. and Lambeck, K., 2007. An inflection in the rate of early mid-Holocene eustatic sea-level rise: A new sea-level curve from Singapore. *Estuarine, Coastal and Shelf Science*, 71(3-4), pp.523-536. <https://doi.org/10.1016/j.ecss.2006.07.004>
- Biswal, T.K., Kundu, B., Anand, M., and Subramanyan, V., 2003. Morphotectonic analysis of the Konkan Coast of Maharashtra and its seismic implication. In: Gupta, H.K. and Gupta, G.D. (eds.), *Earthquake Studies in Peninsular India: Since 1993*. Geological Society of India Memoir 54.
- Bhattacharya, F., 2021. Mid to Late-Holocene relative sea-level fluctuations and palaeoenvironment: Evidences from the southern Saurashtra coast, western India. *Quaternary International*, 599, 62-71. <https://doi.org/10.1016/j.quaint.2020.08.047>
- Bhattacharya, A.K., Kurien, T.K., Krishnanunni, K. and Seiti, D.N., 1979. Geomorphic mapping in parts of Kerala state. *Journal of the Indian Society of Photo-Interpretation and Remote Sensing*, 7(1), 1-9. <https://doi.org/10.1007/BF02991450>
- Billy, J., Robin, N., Hein, C.J., Certain, R. and FitzGerald, D.M., 2015. Insight into the late Holocene sea-level changes in the NW Atlantic from a paraglacial beach-ridge plain south of Newfoundland. *Geomorphology*, 248, 134-146. <https://doi.org/10.1016/j.geomorph.2015.07.033>

- Bjørnsen, M., Clemmensen, L.B., Murray, A. and Pedersen, K., 2008. New evidence of the Littorina transgressions in the Kattegat: Optically Stimulated Luminescence dating of a beach ridge system on Anholt, Denmark. *Boreas*, 37(1), 157-168.
- Bøtter-Jensen, L., Solongo, S., Murray, A.S., Banerjee, D. and Jungner, H., 2000. Using the OSL single-aliquot regenerative-dose protocol with quartz extracted from building materials in retrospective dosimetry. *Radiation Measurements*, 32(5), 841-845. [https://doi.org/10.1016/S1350-4487\(99\)00278-4](https://doi.org/10.1016/S1350-4487(99)00278-4)
- Brooke, B.P., Huang, Z., Nicholas, W.A., Oliver, T.S., Tamura, T., Woodroffe, C.D. and Nichol, S.L., 2019. Relative sea-level records preserved in Holocene beach-ridge strandplains—An example from tropical northeastern Australia. *Marine Geology*, 411, 107-118. <https://doi.org/10.1016/j.margeo.2019.02.005>
- Bruckner H (1989) Late Quaternary shorelines in India. In: D,B,Scott, P.A.Pirazzoli and C.A. Honig (Eds), Late Quaternary Sea Level Correlation and Applications. Kluwer Academic Publishers, Dordrecht. Pp.169-194.
- Bürgmann, R., Rosen, P.A. and Fielding, E.J., 2000. Synthetic aperture radar interferometry to measure Earth's surface topography and its deformation. *Annual review of earth and planetary sciences*, 28(1), 169-209. <https://doi.org/10.1146/annurev.earth.28.1.169>
- Carver, R.E., 1971. *Procedures in Sedimentary Petrology*. Wiley-Interscience, New York.
- Chen, Y.G. and Liu, T.K., 2000. Holocene uplift and subsidence along an active tectonic margin southwestern Taiwan. *Quaternary Science Reviews*, 19(9), 923-930. [https://doi.org/10.1016/S0277-3791\(99\)00076-1](https://doi.org/10.1016/S0277-3791(99)00076-1)
- Choi, K.H., Choi, J.H. and Kim, J.W., 2014. Reconstruction of Holocene coastal progradation on the east coast of Korea based on OSL dating and GPR surveys of beach-foredune ridges. *The Holocene*, 24(1), 24-34. <https://doi.org/10.1177/0959683613515728>
- Chowdhury, S.Q., Fazlul, A.T.M. and Hasan, H.K., 1997. Beachrock in St. Mar'in's Island, Bangladesh: Implications of sea level changes on beachrock cementation. *Marine Geodesy*, 20(1), 89-104. <https://doi.org/10.1080/01490419709388097>
- Clemmensen, L.B. and Nielsen, L., 2010. Internal architecture of a raised beach ridge system (Anholt, Denmark) resolved by ground-penetrating radar investigations. *Sedimentary Geology*, 223(3-4), 281-290. <https://doi.org/10.1016/j.sedgeo.2009.11.014>
- Clemmensen, L.B., Nielsen, L., Bendixen, M. and Murray, A., 2012. Morphology and sedimentary architecture of a beach-ridge system (Anholt, the Kattegat sea): a record of punctuated coastal progradation and sea-level change over the past ~ 1000 years. *Boreas*, 41(3), 422-434. <https://doi.org/10.1111/j.1502-3885.2012.00250.x>
- Costas, S., Ferreira, Ó., Plomaritis, T.A. and Leorri, E., 2016. Coastal barrier stratigraphy for Holocene high-resolution sea-level reconstruction. *Scientific reports*, 6(1), 1-12. <https://doi.org/10.1038/srep38726>
- Čyžienė, J., Korabliova, L., Mikulėnas, V., Minkevičius, V. and Satkūnas, J., 2007, August. Integrated interpretation of geophysical a34araikal34ite radar interferometry data for mapping of neotectonics: a case study of Vilnius City, Lithuania. In Volume of Abstracts (p.8).

- Dabhi, M., Thakkar, A., Chavan, A., Chauhan, G., Bhagora, R., Chauhan, N., Shukla, A.D., Bhandari, S. and Thakkar, M.G., 2021. Mid-late Holocene climatic reconstruction from coastal dunes of the western Kachchh, India. *Quaternary International*. <https://doi.org/10.1016/j.quaint.2021.09.011>
- Daniels DJ (2004) *Ground-penetrating radar* 2nd edn. The Institution of Engineering and Technology, London
- Deshpande, G.G., 1998. *Geology of Maharashtra*. Geological Society of India, Text Book Series 10, 223p.
- Deshraj, T., Koravangatt, D., Ilya, B., Vipul, S. and Rajesh R, N., 2012. Interpretation of dune genesis from sedimentological data and ground penetrating radar (GPR) signatures: a case study from Ashirmata dune field, Mandvi beach, Gujarat, India. *International Journal of Geosciences*, 2012. <http://dx.doi.org/10.4236/ijg.2012.34078>
- Dillenburg, S.R., Barboza, E.G., Rosa, M.L.C., Caron, F. and Sawakuchi, A.O., 2017. The complex prograded Cassino barrier in southern Brazil: Geological and morphological evolution and records of climatic, oceanographic and sea-level changes in the last 7–6 ka. *Marine Geology*, 390, pp.106-119. <https://doi.org/10.1016/j.margeo.2017.06.007>
- Dougherty, A.J. and Dickson, M.E., 2012. Sea level and storm control on the evolution of a chenier plain, Firth of Thames, New Zealand. *Marine Geology*, 307,58-72. <https://doi.org/10.1016/j.margeo.2012.03.003>
- Dougherty, A.J., 2014. Extracting a record of Holocene storm erosion and deposition preserved in the morphostratigraphy of a prograded coastal barrier. *Continental Shelf Research*, 86, 116-131. <https://doi.org/10.1016/j.csr.2013.10.014>
- Dougherty, A.J., Choi, J.H., Turney, C.S. and Dosseto, A., 2019. Optimizing the utility of combined GPR, OSL, and Lidar (GOaL) to extract paleoenvironmental records and decipher shoreline evolution. *Climate of the Past*, 15(1), 389-404. <https://doi.org/10.5194/cp-15-389-2019>
- Durcan, J.A., King, G.E. and Duller, G.A., 2015. DRAC: Dose Rate and Age Calculator for trapped charge dating. *Quaternary Geochronology*, 28, 54-61. <https://doi.org/10.1016/j.quageo.2015.03.012>
- Fairbanks, R.G., 1989. A 17,000-year glacio-eustatic sea level record: influence of glacial melting rates on the Younger Dryas event and deep-ocean circulation. *Nature*, 342(6250), 637-642.
- Fleming, K., Johnston, P., Zwartz, D., Yokoyama, Y., Lambeck, K. and Chappell, J., 1998. Refining the eustatic sea-level curve since the Last Glacial Maximum using far-and intermediate-field sites. *Earth and Planetary Science Letters*, 163(1-4), 327-342.
- Folk, R.L., 1980. *Petrology of Sedimentary Rocks*. Hemphill Publishing Co., Austin, Texas, U.S.A.
- Forbes, D.L., 1994. Paraglacial coasts In: Schwartz, M.L. (Ed.), *Encyclopedia of Coastal Science*. Springer, Dordrecht, 760-762.
- Forte, E., Dossi, M., Pipan, M., Colucci, R.R., 2014. Velocity analysis from common offset GPR data inversion: theory and application to synthetic and real data. *Geophysical Journal International* 197(3):1471-1483. <https://doi.org/10.1093/gji/ggu103>
- GSSI (2015) *Radan user manual: version 7.0* Geophysical Survey Systems Inc, USA

- Gouramanis, C., Switzer, A.D., Bristow, C.S., Pham, D.T., Mauz, B., Hoang, Q.D., Lam, D.D., Lee, Y.S., Soria, J.L.A., Pile, J. and Chi, N.T.K., 2020. Holocene evolution of the Chan May coastal embayment, central Vietnam: Changing coastal dynamics associated with decreasing rates of progradation possibly forced by mid-to late-Holocene sea-level changes. *Geomorphology*, 367, 107273. <https://doi.org/10.1016/j.geomorph.2020.107273>
- Goy, J.L., Zazo, C. and Dabrio, C.J., 2003. A beach-ridge progradation complex reflecting periodical sea-level and climate variability during the Holocene (Gulf of Almeria, Western Mediterranean). *Geomorphology*, 50(1-3), 251-268. [https://doi.org/10.1016/S0169-555X\(02\)00217-9](https://doi.org/10.1016/S0169-555X(02)00217-9)
- Gupta, S.K., 1972. Chronology of the raised beaches and inland coral reefs of the Saurashtra coast. *The Journal of Geology*, 80(3), 357-361.
- Hanamgond, P.T. and Mitra, D., 2008. Evolution of Malvan coast, Konkan, West Coast of India—A case study using remote sensing data. *Journal of Coastal Research*, 24(3), 672-678.
- Hashimi, N.H., Nigam, R., Nair, R.R. and Rajagopalan, G., 1995. Holocene sea level fluctuations on western Indian continental margin: an update. *Jornal Geological Society of India*
- Hede, M.U., Sander, L., Clemmensen, L.B., Kroon, A., Pejrup, M. and Nielsen, L., 2015. Changes in Holocene relative sea-level and coastal morphology: A study of a raised beach ridge system on Samsø, southwest Scandinavia. *The Holocene*, 25(9), 1402-1414. <https://doi.org/10.1177/0959683615585834>
- Hein, C.J., FitzGerald, D.M., de Menezes, J.T., Cleary, W.J., Klein, A.H. and Albernaz, M.B., 2014. Coastal response to late-stage transgression and sea-level highstand. *GSA Bulletin*, 126(3-4), 459-480. <https://doi.org/10.1130/B30836.1>
- Heteren, V.S. and Van de Plassche, O., 1997. Influence of relative sea-level change and tidal-inlet development on barrier-spit stratigraphy, Sandy Neck, Massachusetts. *Journal of Sedimentary Research*, 67(2), 350-363.
- Heteren, V.S., Huntley, D.J., van de Plassche, O. and Lubberts, R.K., 2000. Optical dating of dune sand for the study of sea-level change. *Geology*, 28(5), 411-414.
- Hu, J., Huang, M., Cooksley, G., Duro, J., Arnaud, A., Fruneau, B. and Deffontaines, B., 2006, December. Neotectonic deformation in 38araikwan as deduced from persistent scatterers sar interferometry and geodetic observation. In AGU Fall Meeting Abstracts (Vol. 2006, pp. T33D-0534).
- Houser, C., 2012. Feedback between ridge and swale bathymetry and barrier island storm response and transgression. *Geomorphology*, 173, 1-16. <https://doi.org/10.1016/j.geomorph.2012.05.021>
- Huang, M.H., Hu, J.C., Hsieh, C.S., Ching, K.E., Rau, R.J., Pathier, E., Fruneau, B. and Deffontaines, B., 2006. A growing structure near the deformation front in SW Taiwan as deduced from SAR interferometry and geodetic observation. *Geophysical Research Letters*, 33(12). <https://doi.org/10.1029/2005GL025613>
- Jain, M., Woodcock, N.H. and Tandon, S.K., 1998. Neotectonics of western India: evidence from deformed Quaternary fluvial sequences, Mahi River, Gujarat. *Journal of the Geological Society*, 155(6), 897-901. <https://doi.org/10.1144/gsjgs.155.6.0897>

- Jol, H.M., 2008. Ground penetrating radar theory and applications. Elsevier, UK
- Juyal, N., Pant, R.K. and Somayajulu, R.B.A.B., 1995. Radiometric dating of Late Quaternary sea levels of the Saurashtra coast, western India: an experiment with Oyster and Clam shells. *Memoirs Geological Society of India*, 32, 372-379
- Kale, V.S. and Rajaguru, S.N., 1985. Neogene And Quaternary Transgressional And Regressional History Of The West Coast Of India: An Overview. *Bulletin of the Deccan College Research Institute*, 44, pp.153-167.
- Kakroodi, A.A., Leroy, S.A.G., Kroonenberg, S.B., Lahijani, H.A.K., Alimohammadian, H., Boomer, I. and Goorabi, A., 2015. Late Pleistocene and Holocene sea-level change and coastal paleoenvironment evolution along the Iranian Caspian shore. *Marine Geology*, 361, 111-125. <https://doi.org/10.1016/j.margeo.2014.12.007>
- Kelsey, H.M., 2015. Geomorphological indicators of past sea levels. *Handbook of Sea-Level Research*, 66-82. <https://doi.org/10.1002/9781118452547.ch5>
- Khan, T.M.A., Quadir, D.A., Murty, T.S., Kabir, A., Aktar, F. and Sarker, M.A., 2002. Relative sea level changes in Maldives and vulnerability of land due to abnormal coastal inundation. *Marine Geodesy*, 25(1-2), 133-143. <https://doi.org/10.1080/014904102753516787>
- Kumaran, K.P.N., Shindikar, M. and Limaye, R.B., 2004. Mangrove associated lignite beds of Malvan, Konkan: evidence for higher sea-level during the Late Tertiary (Neogene) along the west coast of India. *Current Science*, 335-340.
- Kunte, P.D. and Wagle, B.G., 2005. The beach ridges of India: a review. *Journal of Coastal Research*, 174-183.
- Lakhote, A., Thakkar, M.G., Kandregula, R.S., Jani, C., Kothiyari, G.C., Chauhan, G. and Bhandari, S., 2021. Estimation of active surface deformation in the eastern Kachchh region, western India: Application of multi-sensor DInSAR technique. *Quaternary International*, 575, 130-140. <https://doi.org/10.1016/j.quaint.2020.07.010>
- Li, Z., Saito, Y., Mao, L., Tamura, T., Song, B., Zhang, Y., Lu, A., Sieng, S., Li, J., 2012. MidHolocene mangrove succession and its response to sea-level change in the upper Mekong River delta, Cambodia. *Quatern. Res.* 78 (2), 386–399.
- Lindhorst, S. and Schutter, I., 2014. Polar gravel beach-ridge systems: Sedimentary architecture, genesis, and implications for climate reconstructions (South Shetland Islands/Western Antarctic Peninsula). *Geomorphology*, 221, 187-203. <https://doi.org/10.1016/j.geomorph.2014.06.013>
- Loveson, V.J. and Rajamanickam, G.V., 1994. Evidences for the phenomena of emergence along southern tamil nadu coast through remote sensing methods. *Glimpses of Tamil Civilization: Articles from the University Quarterly*, Tamil Civilization, 346.
- Loveson, V.J., Rajamanickam, G.V., and Tooley, M.J., 2001. Evidence of quaternary sea level changes and shoreline displacement on the south eastern Coromandal coast of India. In *International Seminar on Quaternary Sea Level Variation, Shoreline Displacement and Coastal Environment* (pp. 85-93).

- Loveson VJ, Gujar AR, Barnwal R, Khare R, Rajamanickam GV 2014a. Gpr studies over the tsunami affected Karaikalkal beach, Tamil Nadu South India. *J Earth Syst Sci* 123(6), 1375-1385. <https://doi.org/10.1007/s12040-014-0463-7>
- Loveson, V.J., Gujar, A.R., Iyer, S.D., Udayaganesan, P., Luis, R.A.A., Gaonkar, S.S., Chithrabhanu, P., Tirodkar, G.M. and Singhvi, A.K., 2014b. Beach dynamics and oscillations of shoreline position in recent years at Miramar Beach, Goa, India: a study from a GPR survey. *Natural hazards*, 73(3), 2089-2106. <https://doi.org/10.1007/s11069-014-1175-7>
- Loveson, V.J. and Nigam, R., 2019. Reconstruction of Late Pleistocene and Holocene sea level curve for the east coast of India. *Journal of the Geological Society of India*, 93(5), 507-514. <https://doi.org/10.1007/s12594-019-1211-z>
- Mann, T., Bender, M., Lorscheid, T., Stocchi, P., Vacchi, M., Switzer, A.D. and Rovere, A., 2019. Holocene sea levels in southeast Asia, Maldives, India and Sri Lanka: the SEAMIS database. *Quaternary Science Reviews*, 219, 112-125. <https://doi.org/10.1016/j.quascirev.2019.07.007>
- Maurya, D.M., Patidar, A.K., Mulchandani, N., Goyal, B., Thakkar, M.G., Bhandari, S., Vaid, S.I., Bhatt, N.P. and Chamyal, L.S., 2005. Need for initiating ground penetrating radar studies along active faults in India: An example from Kachchh. *Current Science*, 88(2), 231-240.
- Maurya, D.M., Goyal, B., Patidar, A.K., Mulchandani, N., Thakkar, M.G. and Chamyal, L.S., 2006. Ground Penetrating Radar imaging of two large sand blow craters related to the 2001 Bhuj earthquake, Kachchh, Western India. *Journal of applied geophysics*, 60(2), pp.142-152. <https://doi.org/10.1016/j.jappgeo.2006.02.001>
- Mazzotti, S., Lambert, T., Van der Kooij, M. and Mainville, A., 2006, December. Coastal subsidence and relative sea-level rise in the Fraser River delta, Greater Vancouver, BC, from a combined CTM-InSAR, GPS, leveling, and tide gauge analysis. In *AGU Fall Meeting Abstracts* (Vol. 2006, pp. G23A-1263).
- McSaveney, M.J., Graham, I.J., Begg, J.G., Beu, A.G., Hull, A.G., Kim, K. and Zondervan, A., 2006. Late Holocene uplift of beach ridges at Turakirae Head, south Wellington coast, New Zealand. *New Zealand Journal of Geology and Geophysics*, 49(3), 337-358. <https://doi.org/10.1080/00288306.2006.9515172>
- Milne, G.A., Gehrels, W.R., Hughes, C.W. and Tamisiea, M.E., 2009. Identifying the causes of sea-level change. *Nature Geoscience*, 2(7), 471-478. <https://doi.org/10.1038/ngeo544>
- Murray, A.S. and Wintle, A.G., 2000. Luminescence dating of quartz using an improved single aliquot regenerative-dose protocol. *Radiation measurements*, 32(1), 57-73. [https://doi.org/10.1016/S1350-4487\(99\)00253-X](https://doi.org/10.1016/S1350-4487(99)00253-X)
- Nair, R.R. 1974. Holocene sea-levels on the Western Continental Shelf of India. *Proceedings of the Indian Academy of Science - Section B* 79, 197-203. <https://doi.org/10.1007/BF03045465>
- Neal, A., Richards, J. and Pye, K., 2003. Sedimentology of coarse-clastic beach-ridge deposits, Essex, southeast England. *Sedimentary Geology*, 162(3-4), 167-198. [https://doi.org/10.1016/S0037-0738\(03\)00136-2](https://doi.org/10.1016/S0037-0738(03)00136-2)
- Neal, A., 2004. Ground-penetrating radar and its use in sedimentology: principles, problems and progress. *Earth-science reviews*, 66(3-4), 261-330. <https://doi.org/10.1016/j.earscirev.2004.01.004>

- Nielsen, A., Murray, A.S., Pejrup, M. and Elberling, B., 2006. Optically stimulated luminescence dating of a Holocene beach ridge plain in Northern Jutland, Denmark. *Quaternary Geochronology*, 1(4), 305-312. <https://doi.org/10.1016/j.quageo.2006.03.001>
- Nielsen, L. and Clemmensen, L.B., 2009. Sea-level markers identified in ground-penetrating radar data collected across a modern beach ridge system in a microtidal regime. *Terra Nova*, 21(6), 474-479. <https://doi.org/10.1111/j.1365-3121.2009.00904.x>
- Nielsen, L., Bendixen, M., Kroon, A., Hede, M.U., Clemmensen, L.B., Weßling, R. and Elberling, B., 2017. Sea-level proxies in Holocene raised beach ridge deposits (Greenland) revealed by ground-penetrating radar. *Scientific reports*, 7(1), 1-8. <https://doi.org/10.1038/srep46460>
- Oliver, T.S., Murray-Wallace, C.V. and Woodroffe, C.D., 2020. Holocene shoreline progradation and coastal evolution at Guichen and Rivoli Bays, southern Australia. *The Holocene*, 30(1), 106-124. <https://doi.org/10.1177/0959683619875815>
- Otvos, E.G., 2000. Beach ridges—definitions and significance. *Geomorphology*, 32(1-2), 83-108. [https://doi.org/10.1016/S0169-555X\(99\)00075-6](https://doi.org/10.1016/S0169-555X(99)00075-6)
- Pant, R.K., Juyal, N., 1993. Late Quaternary coastal instability and sea level changes: new evidence from Saurashtra coast, Western India. *Zeitschrift für Geomorphologie N.F.* 37, 29–40.
- Porat, N., 2006. Use of magnetic separation for purifying quartz for luminescence dating. *Ancient TL*, 24(2), 33-36.
- Powar, K.B., 1993. Geomorphological evolution of Konkan Coastal Belt and adjoining Sahyadri Uplands with reference of Quaternary uplift. *Current science*, 64(11-12), 793-796.
- Prasad, P. and Loveson, V.J., 2020. Signature of buried channels as deduced from subsurface GPR survey at Southwest coast of Tamil Nadu, India. *Arabian Journal of Geosciences*, 13, 1-12. <https://doi.org/10.1007/s12517-020-05439-y>
- Prasad, P., Loveson, V.J., Kotha, M. and Yadav, R., 2020. Application of machine learning techniques in groundwater potential mapping along the west coast of India. *GIScience & Remote Sensing*, 57(6), 735-752. <https://doi.org/10.1080/15481603.2020.1794104>
- Prasad, P., Loveson, V.J. and Kotha, M., 2023. Probabilistic coastal wetland mapping with integration of optical, SAR and hydro-geomorphic data through stacking ensemble machine learning model. *Ecological Informatics*, 77, 102273.
- Psuty, N.P., 1965. Beach-ridge development in Tabasco, Mexico 1. *Annals of the Association of American Geographers*, 55(1), 112-124.
- Psuty, N.P., 1967. *The Geomorphology of Beach-ridges in Tabasco, Mexico*: Baton Rouge, LA.
- Ramasamy, S.M., 1989. Morpho-tectonic evolution of east and west coasts of Indian peninsula.
- Ramos, F.L.G., Landau, L., De Miranda, F.P. and da Silva, C.L., 2010. Use of Information Derived from Radar Remote Sensing (RADARSAT-1) Interferometry and SRTM MOSAIC) for Mapping Neotectonic Activities in the REgion of Manaus City (Amazonas State. *ESA Special Publication*, 677, p36.

- Rémillard, A.M., Buylaert, J.P., Murray, A.S., St-Onge, G., Bernatchez, P. and Héту, B., 2015. Quartz OSL dating of late Holocene beach ridges from the Magdalen Islands (Quebec, Canada). *Quaternary Geochronology*, 30, 264-269. <https://doi.org/10.1016/j.quageo.2015.03.013>
- Ribolini, A., Aguirre, M., Baneschi, I., Consoloni, I., Fucks, E., Isola, I., Mazzarini, F., Pappalardo, M., Zanchetta, G. and Bini, M., 2011. Holocene beach ridges and coastal evolution in the Cabo Raso bay (Atlantic Patagonian coast, Argentina). *Journal of Coastal Research*, 27(5), 973-983. <https://doi.org/10.2112/JCOASTRES-D-10-00139.1>
- Sander, L., Hede, M.U., Fruergaard, M., Nielsen, L., Clemmensen, L.B., Kroon, A., Johannessen, P.N., Nielsen, L.H. and Pejrup, M., 2016. Coastal lagoons and beach ridges as complementary sedimentary archives for the reconstruction of Holocene relative sea-level changes. *Terra Nova*, 28(1), 43-49. <https://doi.org/10.1111/ter.12187>
- Shah-Hosseini, M., Ghanavati, E., Morhange, C., Beni, A.N., Lahijani, H.A. and Hamzeh, M.A., 2018. The evolution of Chabahar beach ridge system in SE Iran in response to Holocene relative sea level changes. *Geomorphology*, 318, 139-147. <https://doi.org/10.1016/j.geomorph.2018.06.009>
- Shan, X., Yu, X., Clift, P.D., Tan, C., Li, S., Wang, Z. and Su, D., 2016. Ground-penetrating radar study of beach-ridge deposits in Huangqihai Lake, North China: the imprint of washover processes. *Frontiers of Earth Science*, 10(1), 183-194. [DOI 10.1007/s11707-015-0501-z](https://doi.org/10.1007/s11707-015-0501-z)
- Sharma, S., Chauhan, G., Shukla, A.D., Nambiar, R., Bhushan, R., Desai, B.G., Pandey, S., Dabhi, M., Bhandari, S., Bhosale, S. and Lakhote, A., 2021. Causes and implications of Mid-to Late Holocene relative sea-level change in the Gulf of Kachchh, western India. *Quaternary Research*, 100, 98-121. <https://doi.org/10.1017/qua.2020.86>
- Shennan, I., 1986. Flandrian sea-level changes in the Fenland. II: Tendencies of sea-level movement, altitudinal changes, and local and regional factors. *Journal of Quaternary Science*, 1(2), 155-179. <https://doi.org/10.1002/jqs.3390010205>
- Shukla, S.B., Patidar, A.K. and Bhatt, N., 2008. Application of GPR in the study of shallow subsurface sedimentary architecture of Modwa spit, Gulf of Kachchh. *Journal of earth system science*, 117(1), 33-40. <https://doi.org/10.1007/s12040-008-0010-5>
- Snead, R.E., 1982. *Coastal Landforms and Surface Features*. Stroudsburg, Pennsylvania: Hutchinson Ross.
- Souza, P.E., Sohbati, R., Murray, A.S., Clemmensen, L.B., Kroon, A. and Nielsen, L., 2021. Optical dating of cobble surfaces determines the chronology of Holocene beach ridges in Greenland. *Boreas*, 50(2), 606-618. <https://doi.org/10.1111/bor.12507>
- Sridhar, A. and Patidar, A., 2005. Ground penetrating radar studies of a point-bar in the Mahi River Basin, Gujarat. *Current Science*, 183-189.
- Storms, J.E. and Kroonenberg, S.B., 2007. The impact of rapid sea level changes on recent Azerbaijan beach ridges. *Journal of Coastal Research*, 23(2), 521-527. <https://doi.org/10.2112/05-0622.1>
- Subrahmanya, K.R., 1996. Tectonic, eustatic and isostatic changes along the Indian coast. In *Sea Level Rise and Coastal Subsidence: Causes, Consequences, and Strategies* (pp. 193-203). Dordrecht: Springer Netherlands.

- Subrahmanya, K.R., 1998. Tectono-magmatic evolution of the west coast of India. *Gondwana research*, 1(3-4), 319-327.
- Sukhtankar, R.K. and Pandian, R.S., 1990. Evaluation of sea-level rise on the shore zone areas of the Maharashtra coast. *Sea Level Variation and Its Impact on Coastal Environment*. Thanjavur, India: Tamil University, pp.329-338.
- Tamura, T., 2012. Beach ridges and prograded beach deposits as palaeoenvironment records. *Earth-Science Reviews*, 114(3-4), 279-297. <https://doi.org/10.1016/j.earscirev.2012.06.004>
- Tandale, T.D., 1993. Coastal environ of Maharashtra—Evolution and human activities (aided with satellite remote sensing). *Journal of the Indian Society of Remote Sensing*, 21(2), 59-65. <https://doi.org/10.1007/BF02996343>
- Tanner, W.F., 1995. Origin of beach ridges and swales. *Marine Geology*, 129(1-2), 149-161. [https://doi.org/10.1016/0025-3227\(95\)00109-3](https://doi.org/10.1016/0025-3227(95)00109-3)
- Taylor, M. and Stone, G.W., 1996. Beach-ridges: a review. *Journal of Coastal Research*, 612-621.
- Trenhaile, A.S., 2010. The effect of Holocene changes in relative sea level on the morphology of rocky coasts. *Geomorphology*, 114(1-2), 30-41. <https://doi.org/10.1016/j.geomorph.2009.02.003>
- Tzanis, A., 2010 matGPR Release 2: A freeware MATLAB® package for the analysis & interpretation of common and single offset GPR data. *FastTimes* 15(1), 17-43.
- Verma, K.K. and Mathur, U.B., 1979. Quaternary sea-level changes along west coast of India. *Geol. Surv. India, Misc. Publ*, (45), 263-272.
- Wells, L.E., 1996. The Santa beach ridge complex: sea-level and progradational history of an open gravel coast in central Peru. *Journal of Coastal Research*, -17.
- Wagle, B.G., Vora, K.H., Karisiddaiah, S.M., Veerayya, M. and Almeida, F., 1994. Holocene submarine terraces on the western continental shelf of India; Implications for sea-level changes. *Marine Geology*, 117(1-4), 207-225.
- Wang, Z., Zhuang, C., Saito, Y., Chen, J., Zhan, Q. and Wang, X., 2012. Early mid-Holocene sealevel change and coastal environmental response on the southern Yangtze delta plain, China: implications for the rise of Neolithic culture. *Quaternary Science Reviews*, 35, 51-62. <https://doi.org/10.1016/j.quascirev.2012.01.005>
- Wang, Z., Zhan, Q., Long, H., Saito, Y., Gao, X., Wu, X., Li, L.I.N. and Zhao, Y., 2013. Early to mid-Holocene rapid sea-level rise and coastal response on the southern Yangtze delta plain, China. *Journal of Quaternary Science*, 28(7), 659-672. <https://doi.org/10.1002/jqs.2662>
- Xiong, H., Zong, Y., Qian, P., Huang, G. and Fu, S., 2018. Holocene sea-level history of the northern coast of South China Sea. *Quaternary Science Reviews*, 194, 12-26. <https://doi.org/10.1016/j.quascirev.2018.06.022>
- Williams, M., Dunkerley, D., Deckker, P.D., Kershaw, P., Chappell, J., 1998. *Quaternary Environments*. Oxford University Press, New York..

Wu, P.C., Wei, M. and D'Hondt, S., 2022. Subsidence in coastal cities throughout the world observed by InSAR. *Geophysical Research Letters*, 49(7), p.e2022GL098477. <https://doi.org/10.1029/2022GL098477>

List of captions for figures

- Figure 1** (a) Location of the study site on the central west coast of India; (b) Sentinel-2 satellite image of the area; (c) geomorphology map displaying the several landforms around the study site; (d) lithology map; (e) high resolution Google earth image showing the GPR profile (black line) along the ridge and swale topography and red dots represent the OSL sample locations
- Figure 2** Workflow in SNAP using Sentinel-1 SLC images for the displacement map generation between March, 2017 to March, 2020
- Figure 3** Displacement map of the coastal area and the Western Ghats region. The study site is located upper left corner. The Western Ghats region shows upliftment and coastal sectors indicate stable to subsidence
- Figure 4** (a) Elevation above mean sea-level along the GPR transect from landward to seaward. The topographic profile shows sequential topographic highs and lows represent ridges (R-1, R-2, R3, and R4) and swales (S-1, S-2, S-3, and S-4) respectively, (b) beach profile shows elevations of the present berm and beachdune boundary which used in modern analogs
- Figure 5** GPR data collected from the beach ridges (R-1, R-2, and R-3). Yellow hyperbolas representing diffraction hyperbolae. Red lines refer the radar facies. Three radar facies such as Rf1, Rf2, and Rf3 represent the aeolian, beachface and shoreface deposits, respectively. Two radar surfaces (black dash line) demarcated based on patterns of radar facies (Rf1, Rf2, and Rf3) and velocity of the radar waves. The yellow and blue circles represent the dune-beach and berm markers, respectively. The red circles indicate the location of OSL sample at the depths of 1 m, 1.5 m, and 2 m from the surface, at the same location sediment sample taken for texture analysis. Vertical rectangles are the obstacles like roads and fences. The water table (during summer, it falls below 4 m) has not been identified due to the high attenuation beyond 4 m depth. Vertical exaggeration is 1:2 (See the text for details)
- Figure 6** Swales (S-1, S-2, S-3) showing multiple horizontal ringing and few seaward dipping radar facies. Vertical exaggeration is 1:2. (See the text for details)
- Figure 7** Present beach ridge (R-4) of the area showing both landward and seaward dipping pattern. It differs from the paleo beach ridges due to the saltwater intrusion, lower in elevation and therefore closer to water table and thus the signal is attenuated more. Vertical exaggeration is 1:2
- Figure 8** Attenuation of radar waves in beach ridges and swales. The high mean and median attenuation with best fitting exponential and power law decay curve at ridges (R-1, R-2, R-3) while the low mean and median attenuation with best fitting exponential and power law decay curve at swales (S-1, S-2, S-4)

- Figure 9** Velocity in the ridges (R-1, R-2, R-3) are maximum because of different stratigraphic pattern whereas velocity in swale (S-1, S-2, S-4) are less and mixed type due to less radar wave penetration. The blue colour indicates the higher velocity contrast in the layer, whereas the grey colour indicates the lower velocity contrast in the layer.
- Figure 10** The profile running across the beach ridge and swale showing the progradation rates based on the OSL ages and distance
- Figure 11** Representation of the sea-level indicator points (dune-beach contact and berm) and their elevations, ages, and distances. Relationship between (a) distance and elevation, (b) distance and age with linear regression, (c) age and relative mean sea-level with errors show fall of relative sea-level
- Figure 12** Comparing sea-level data of different coast of India with the present study. The trend (black line) of sea-level is from 1 to 2 m based on sedimentological and geomorphological evidences
- Figure 13** Conceptual sketch of ridge and swale landform evolution at different stages by sea-level change in the central west coast of India based on topographic data, radar facies and OSL ages (See the text for details)

List of captions for tables

Table 1 Grain size analysis at different depths of beach ridges and swales

Table 2 Summary of OSL measurement details including samples, depth, water content, number of aliquots used (N), radioactivity details, over dispersion (OD), dose rate, central age model (CAM) equivalent dose (De), and ages of beach ridges of Central west coast of India.

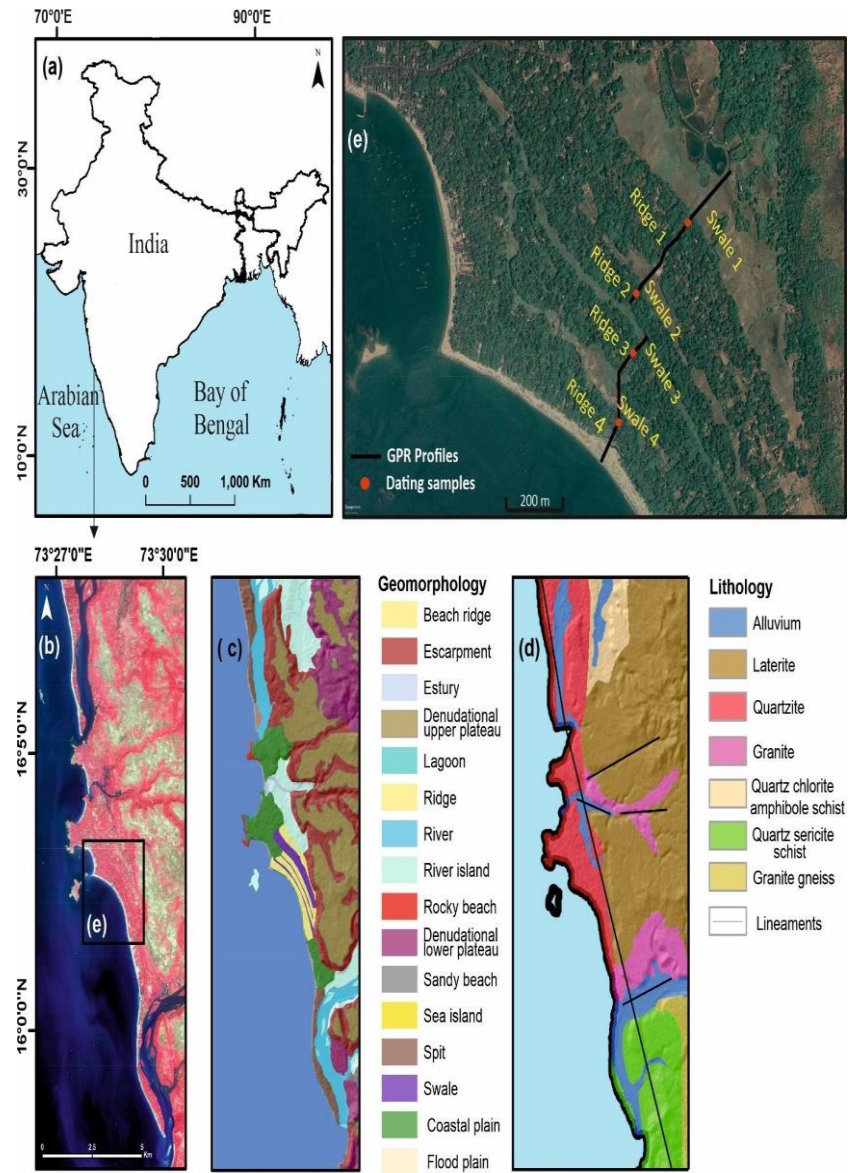


Figure 1

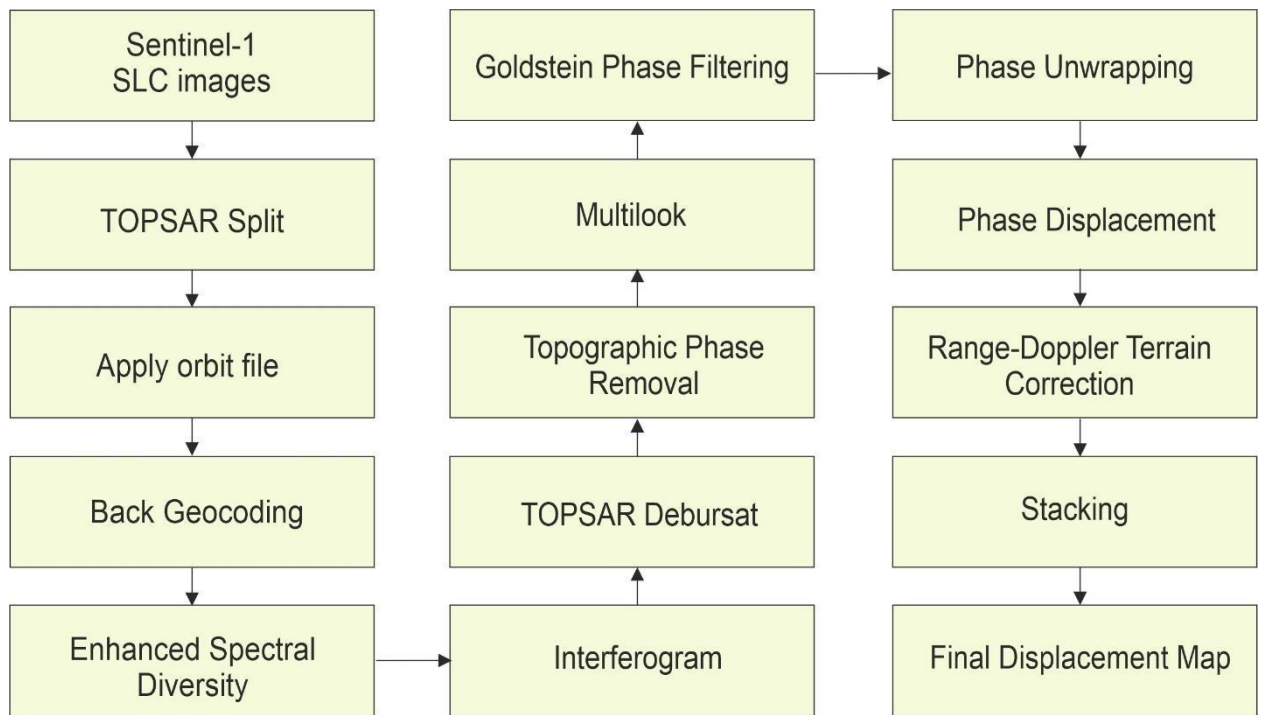


Figure 2

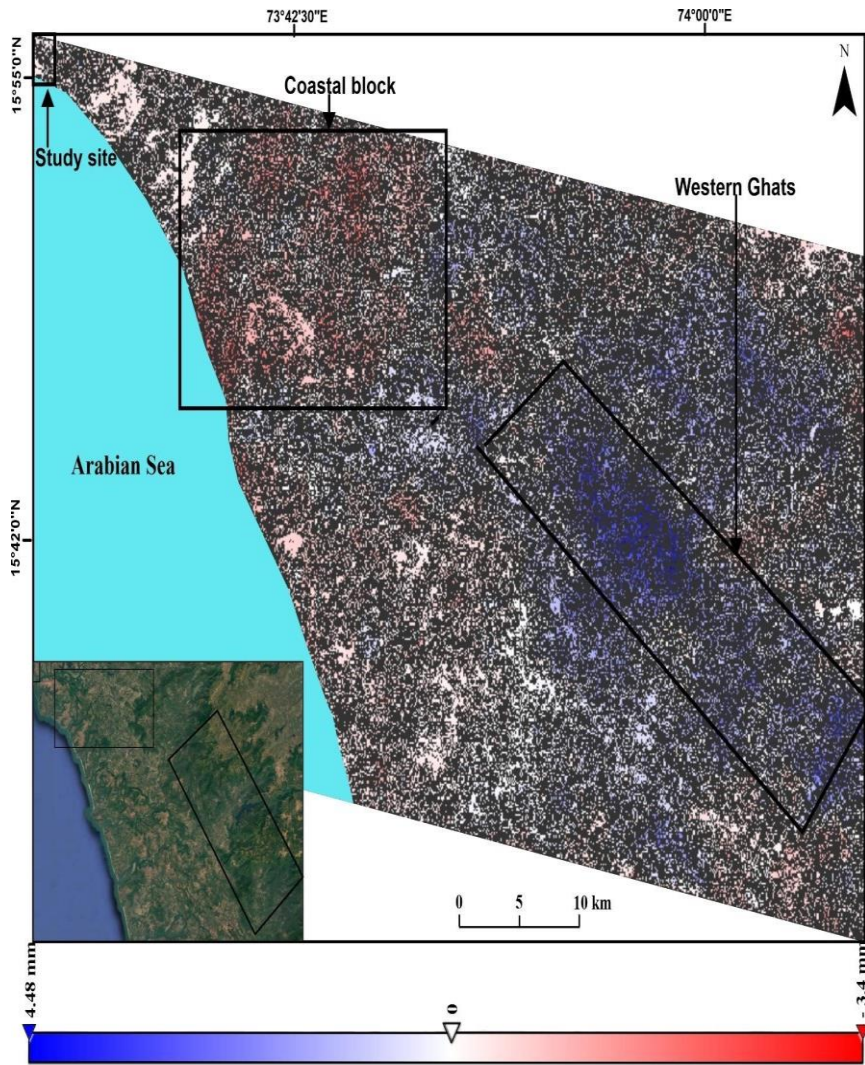


Figure 3

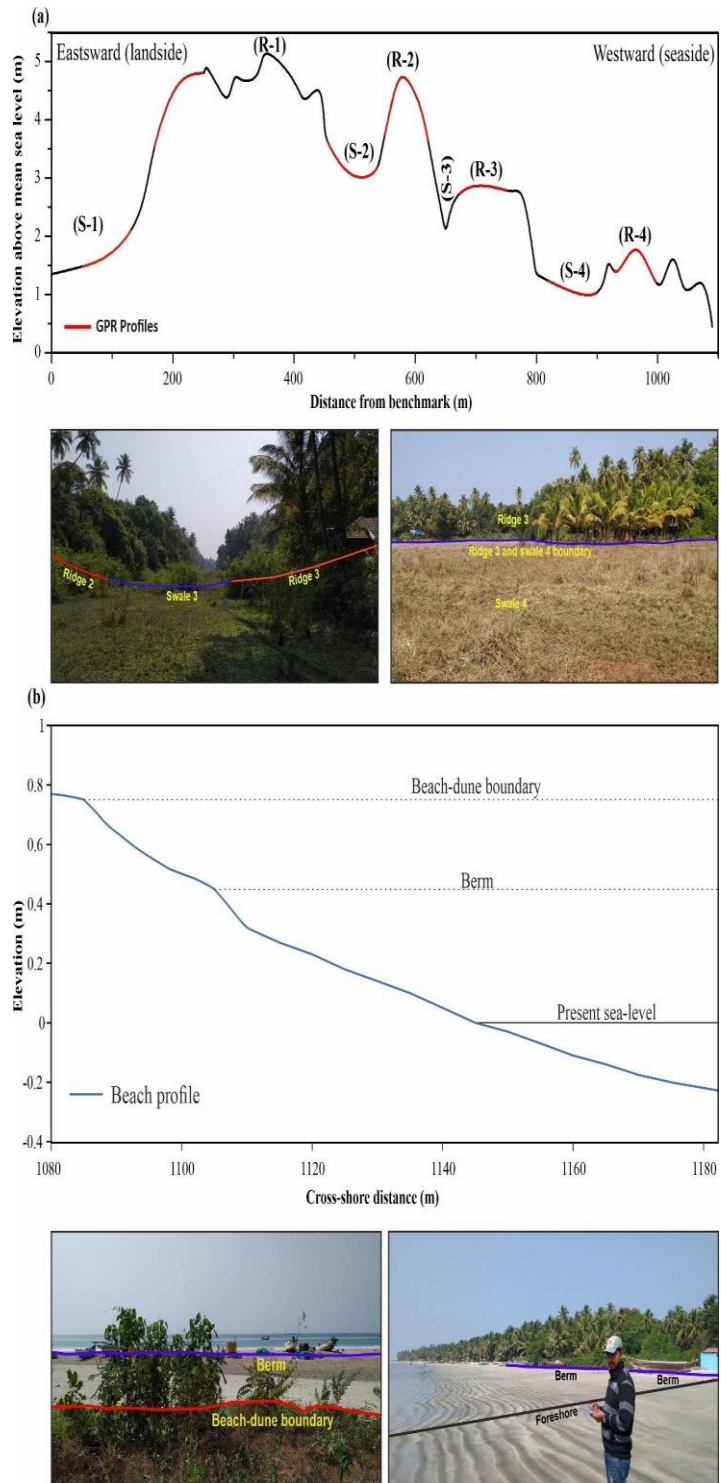


Figure 4

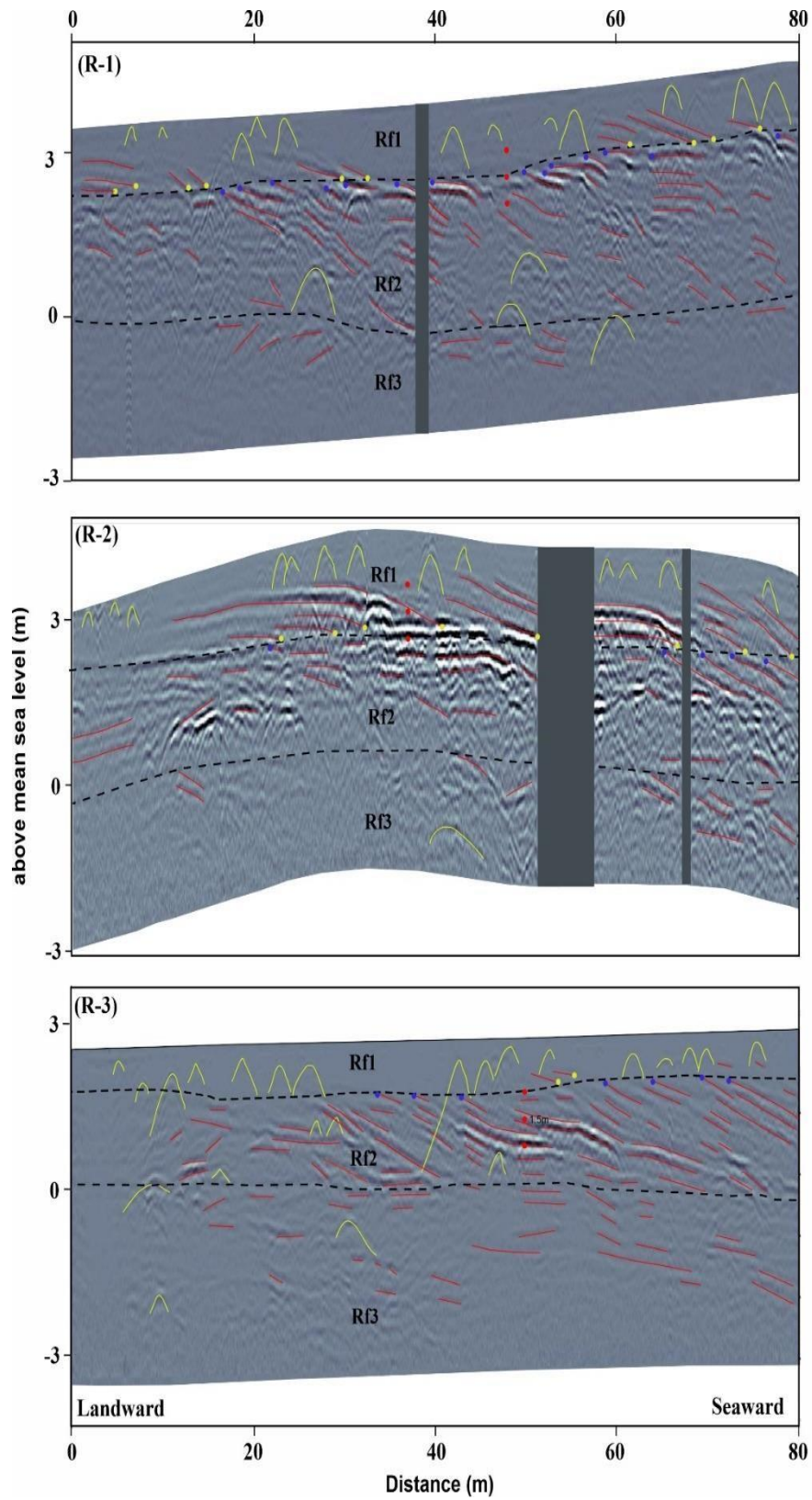


Figure 5

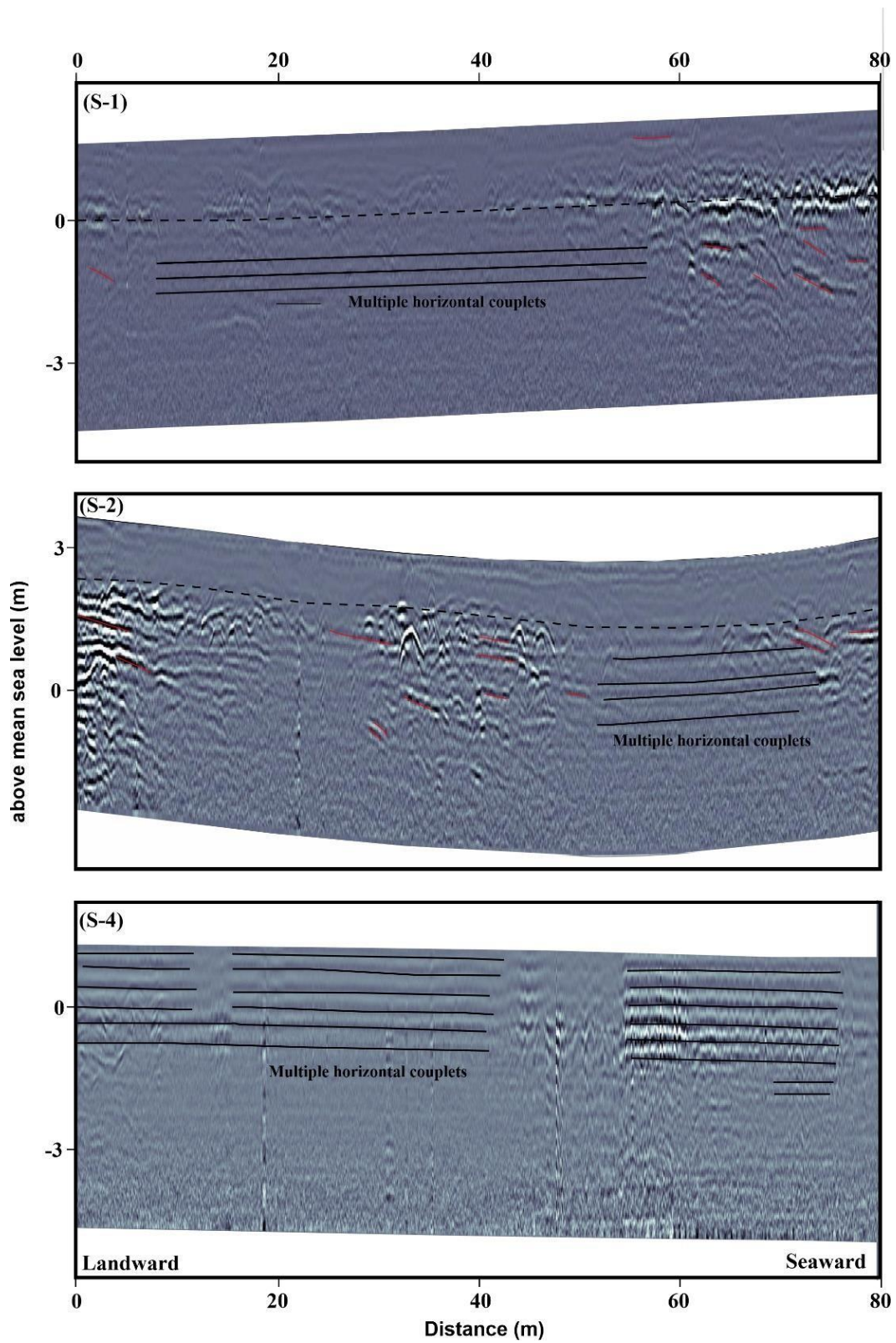


Figure 6

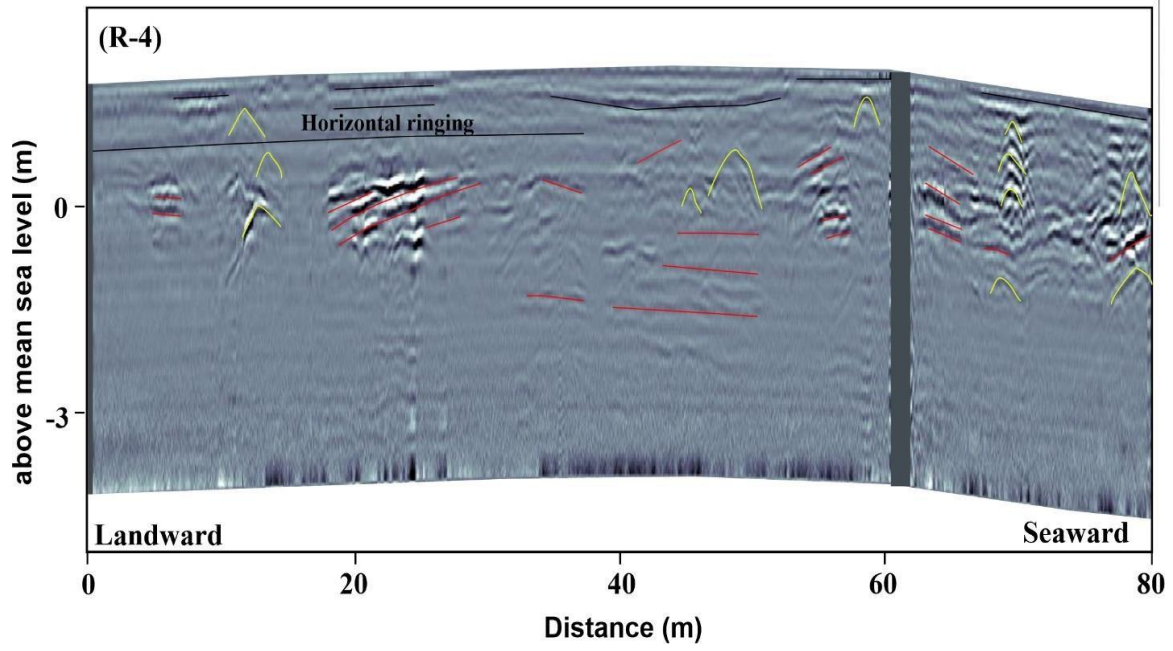


Figure 7

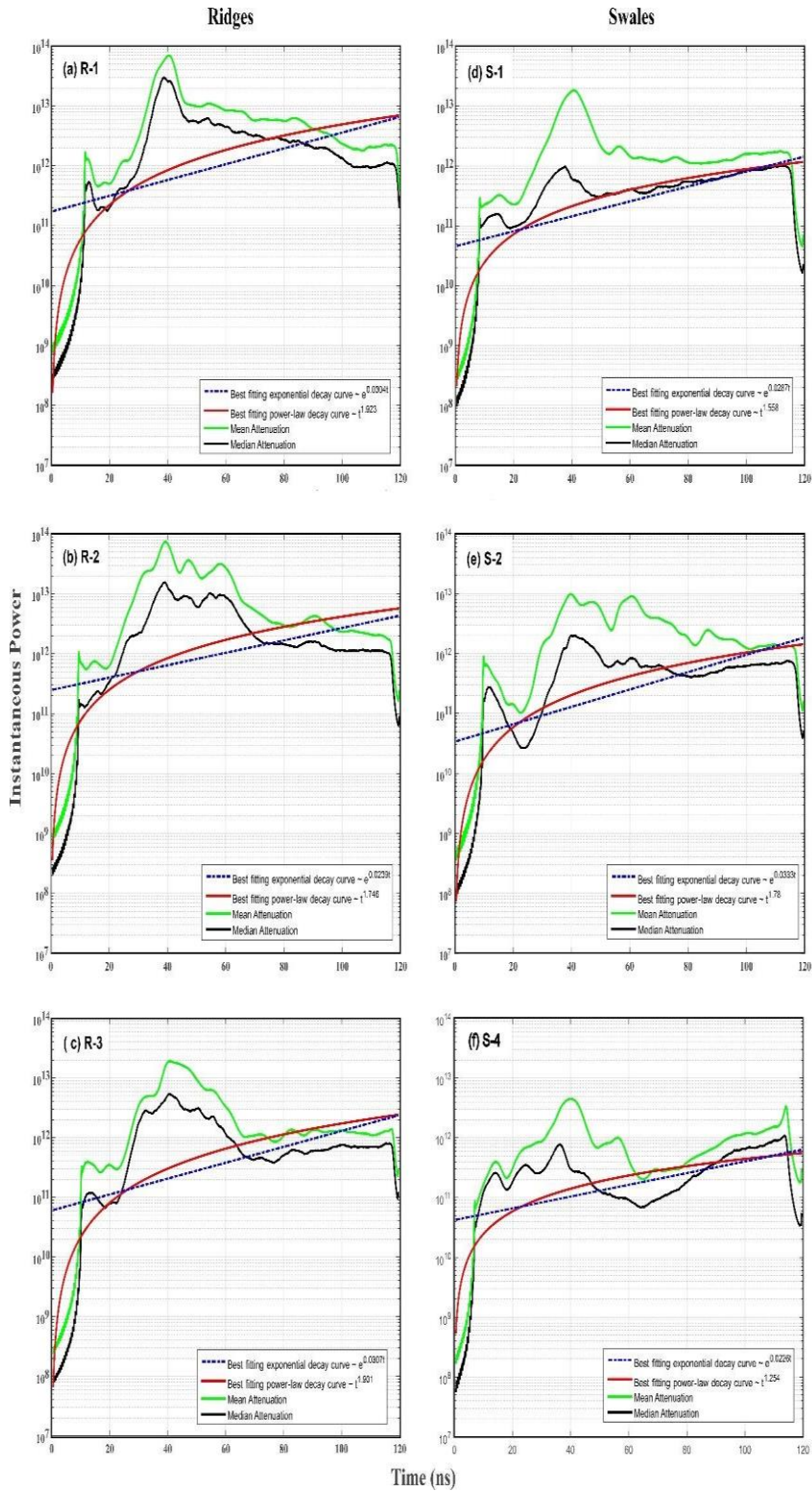


Figure 8

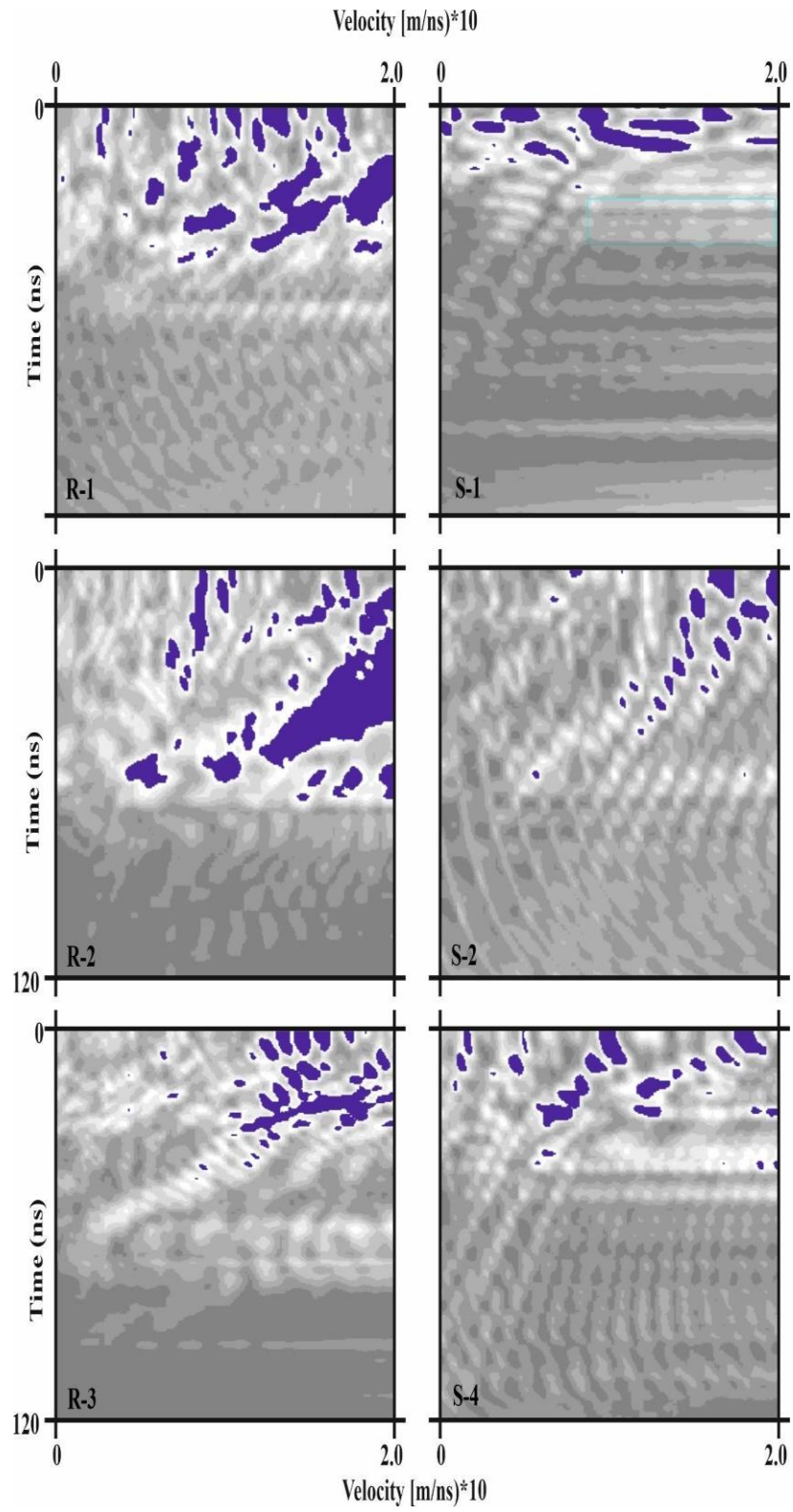


Figure 9

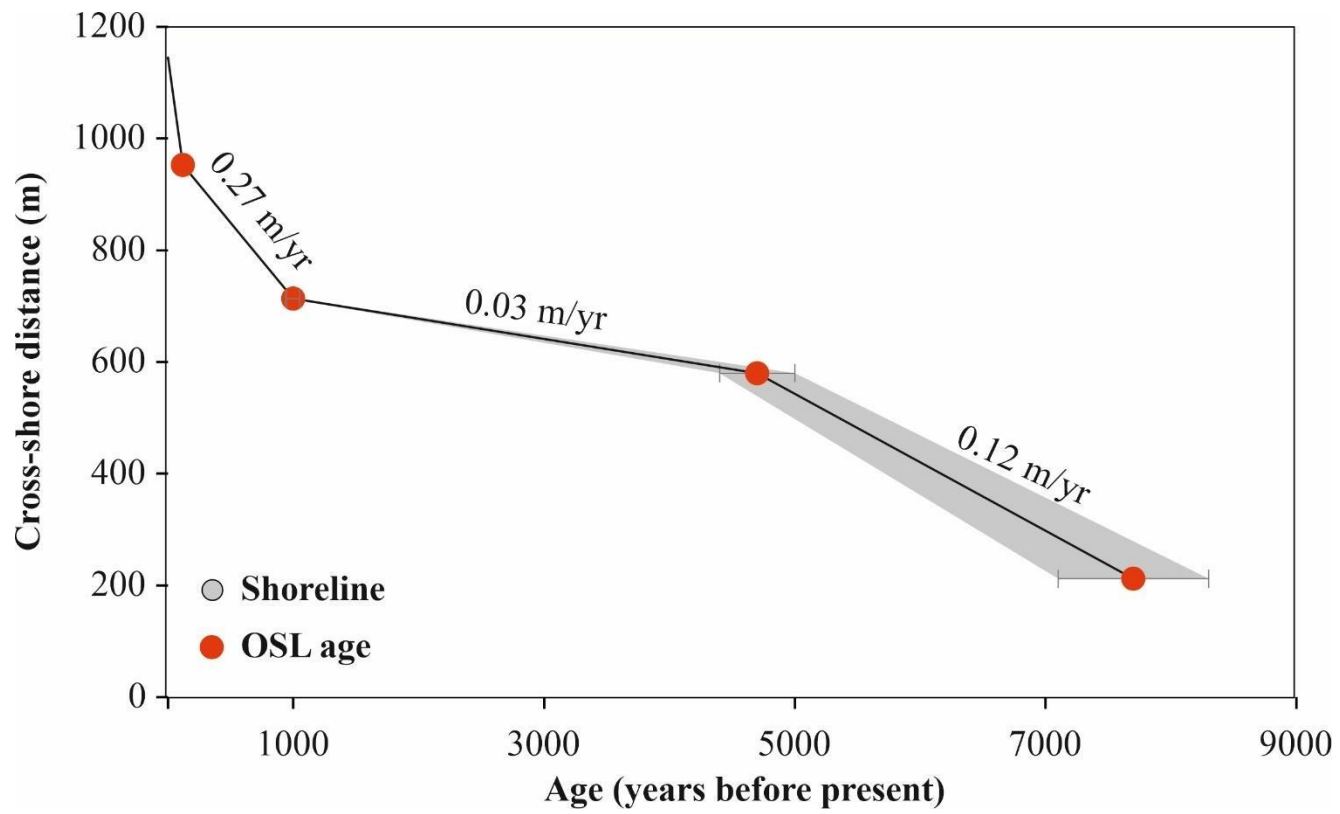


Figure 10

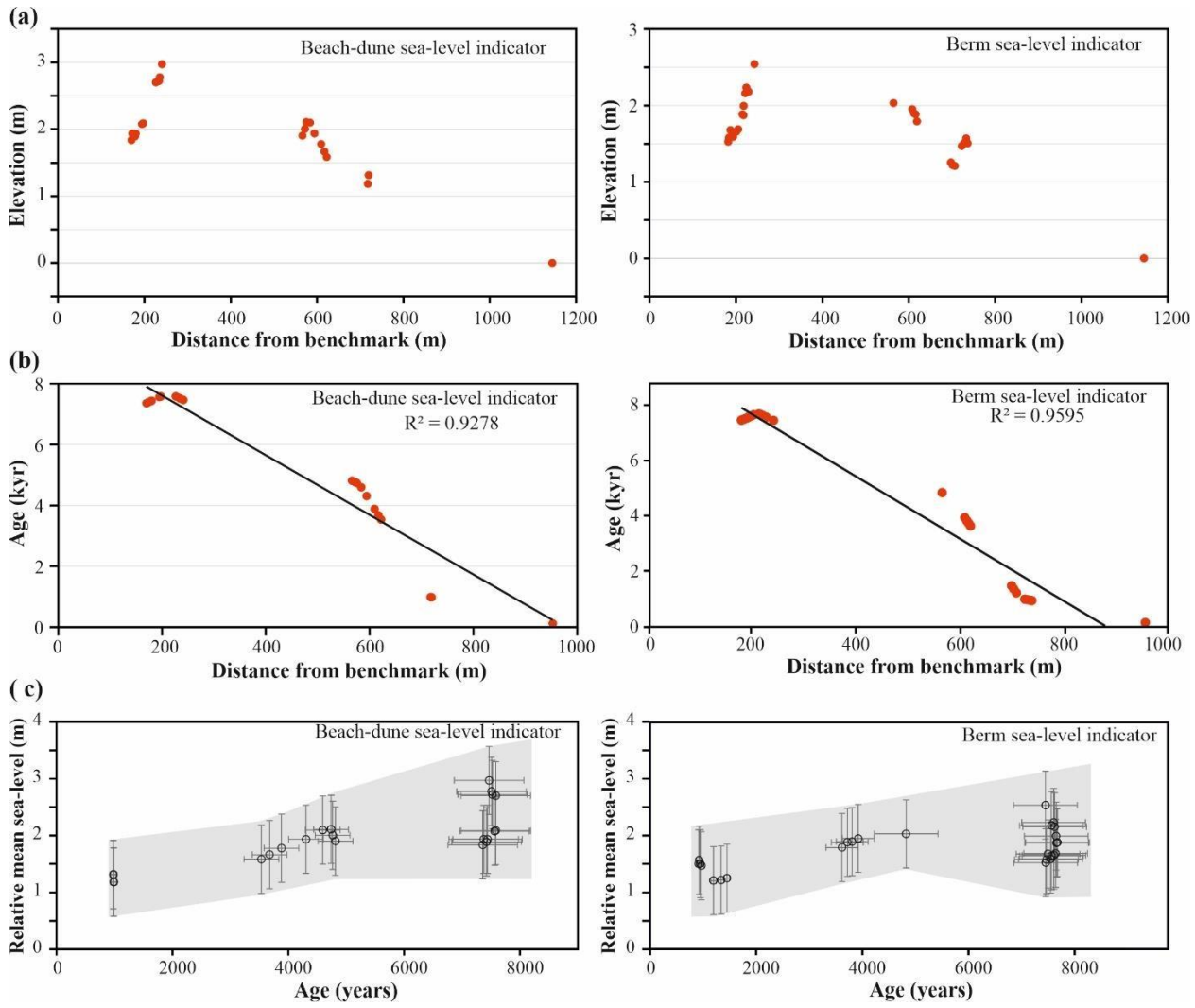


Figure 11

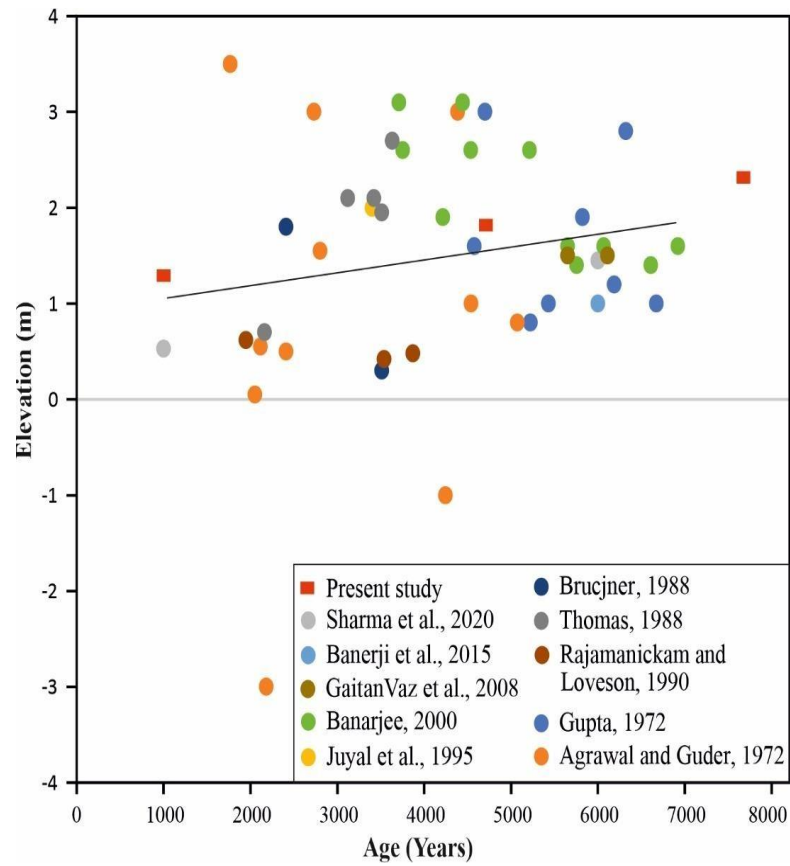


Figure 12

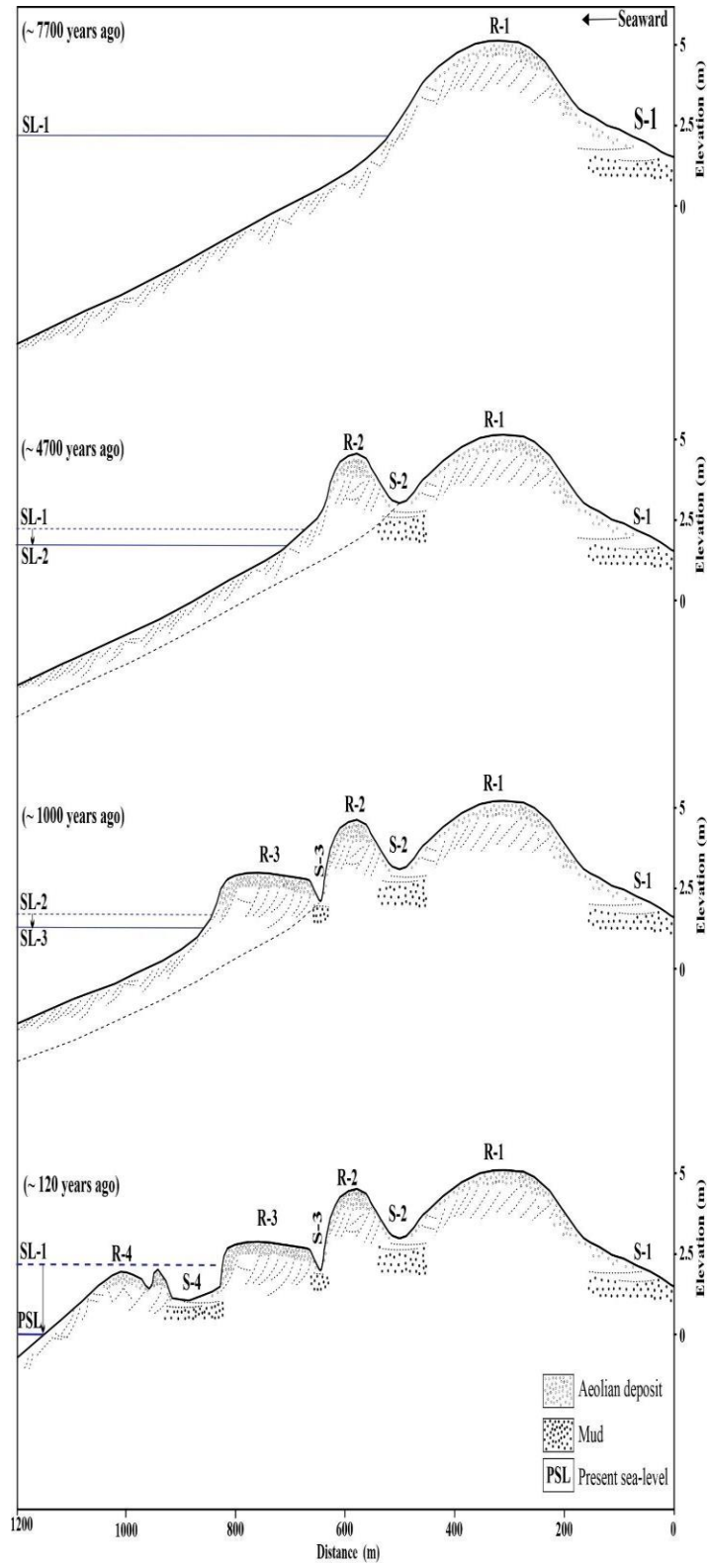


Figure 13

Table 1

Grain size analysis at different depths of beach ridges and swales.

Ridge/swale	Depth (m)	<63 μm (%)	63–125 μm (%)	125–250 μm (%)	250–500 μm (%)	500–1000 μm (%)	>1000 μm (%)
R-1	0.2	0.75	3.00	52.11	42.25	0.67	1.23
	0.5	1.04	1.73	55.06	41.77	0.36	0.04
	1.0	0.26	4.08	62.99	32.39	0.24	0.03
	1.5	1.39	9.37	66.37	22.82	0.05	0.01
	2.0	2.54	3.77	81.98	11.69	0.03	0.00
	Mean	1.19	4.39	63.70	30.18	0.27	0.26
R-2	0.2	0.58	2.57	46.88	49.90	0.07	0.00
	0.5	1.75	4.48	45.57	48.16	0.04	0.00
	1.0	0.59	5.72	60.50	33.18	0.00	0.00
	1.5	1.03	3.66	44.67	50.63	0.01	0.00
	2.0	0.52	5.70	43.26	49.69	0.68	0.14
	Mean	0.90	4.43	48.17	46.31	0.16	0.03
R-3	0.6	1.55	8.13	87.46	2.86	0.00	0.00
	1.0	1.77	7.14	88.85	2.24	0.00	0.00
	1.5	1.22	11.49	84.68	2.54	0.08	0.00
	2.0	0.87	13.92	84.55	0.66	0.00	0.00
	Mean	1.35	10.17	86.39	2.07	0.02	0.00
R-4	0.6	2.34	18.53	73.96	5.17	0.00	0.00
	0.8	4.52	15.57	79.27	0.64	0.00	0.00
	1.0	3.82	15.97	78.87	1.34	0.00	0.00
	Mean	3.56	16.69	77.37	2.38	0.00	0.00
S-1	0.2	5.50	10.79	47.16	35.59	1.15	0.00
	0.6	7.00	11.10	49.76	30.59	1.55	0.00
	0.8	9.57	5.48	52.12	31.74	1.08	0.00
	Mean	7.36	9.12	49.68	32.64	1.26	0.00
S-2	0.3	6.19	3.12	68.05	21.55	1.08	0.00
	0.5	7.85	2.20	56.82	33.14	0.00	0.00
	1.0	10.42	7.59	52.40	29.28	0.32	0.00
	Mean	8.15	4.30	59.08	27.99	0.46	0

Table 2Summary of OSL measurement details including samples, depth, water content, number of aliquots used (N), radioactivity details, over dispersion (OD), dose rate, central age model (CAM) equivalent dose (D_e), and ages of beach ridges of Central west coast of India.

Sample code	Depth (cm)	Water content (%)	N	U (ppm)	Th (ppm)	K (%)	OD (%)	Dose rate (Gy. ka^{-1})	CAM D_e (Gy)	Age (ka)	Ridge no.
R1D1	100	26.8	24	0.59 \pm 0.04	2.06 \pm 0.15	0.12 \pm 0.01	0	0.48 \pm 0.02	3.79 \pm 0.11	7.9 \pm 0.4	1
R1D1.5	150	28.1	24	1.67 \pm 0.06	5.69 \pm 0.25	0.04 \pm 0.01	4.8 \pm 0.3	0.78 \pm 0.023	6.00 \pm 0.41	7.7 \pm 0.6	1
R1D2	200	28.3	24	0.66 \pm 0.05	2.02 \pm 0.19	0.07 \pm 0.01	3 \pm 0.3	0.42 \pm 0.02	3.69 \pm 0.19	8.7 \pm 0.6	1
R2D1	100	25.7	24	1.31 \pm 0.05	4.91 \pm 0.22	0.21 \pm 0.01	0	0.83 \pm 0.02	3.69 \pm 0.15	4.5 \pm 0.2	2
R2D1.5	150	26.2	24	1.2 \pm 0.07	5.4 \pm 0.25	0.22 \pm 0.01	0	0.83 \pm 0.02	3.38 \pm 0.13	4.1 \pm 0.2	2
R2D2	200	27.7	24	1.08 \pm 0.06	3.9 \pm 0.22	0.19 \pm 0.01	3 \pm 0.3	0.69 \pm 0.02	3.25 \pm 0.18	4.7 \pm 0.3	2
R3D1	100	28.1	24	0.66 \pm 0.05	1.76 \pm 0.18	0.69 \pm 0.02	0	0.90 \pm 0.03	0.93 \pm 0.03	1.0 \pm 0.05	3
R3D1.5	150	31.5	24	0.74 \pm 0.05	1.1 \pm 0.19	0.36 \pm 0.01	5.2 \pm 0.4	0.61 \pm 0.02	0.72 \pm 0.06	1.2 \pm 0.1	3
R3D2	200	26.9	24	0.61 \pm 0.05	2.51 \pm 0.2	0.90 \pm 0.02	0	1.08 \pm 0.03	0.98 \pm 0.03	0.91 \pm 0.04	3
R4D0.8	80	26.4	24	0.98 \pm 0.06	3.32 \pm 0.22	0.34 \pm 0.01	7.2 \pm 0.6	0.79 \pm 0.03	0.10 \pm 0.01	0.12 \pm 0.01	4